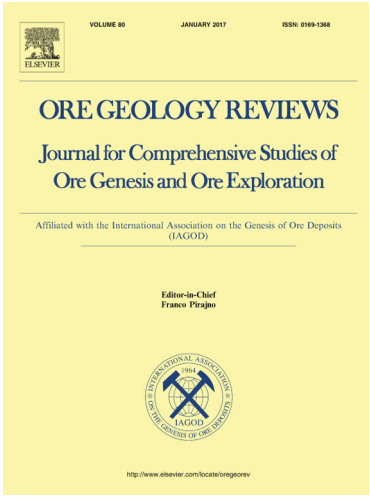

Composition and Origin of Rare-Metal (Nb–Ta, REE) and Sulfide Mineralization in Magnesiocarbonatites from the Yenisei Ridge, Central Siberia

V.V. Vrublevskii, O.V. Bukharova, T.S. Nebera, V.L. Sveshnikova

PII: S0169-1368(18)30570-5
DOI: https://doi.org/10.1016/j.oregeorev.2019.102949
Article Number: 102949
Reference: OREGEO 102949

To appear in: *Ore Geology Reviews*

Received Date: 4 July 2018
Revised Date: 7 May 2019
Accepted Date: 28 May 2019

Please cite this article as: V.V. Vrublevskii, O.V. Bukharova, T.S. Nebera, V.L. Sveshnikova, Composition and Origin of Rare-Metal (Nb–Ta, REE) and Sulfide Mineralization in Magnesiocarbonatites from the Yenisei Ridge, Central Siberia, *Ore Geology Reviews* (2019), doi: https://doi.org/10.1016/j.oregeorev.2019.102949

Composition and Origin of Rare-Metal (Nb–Ta, REE) and Sulfide Mineralization in Magnesiocarbonatites from the Yenisei Ridge, Central Siberia

V.V. Vrublevskii[a], O.V. Bukharova[a], T.S. Nebera[a], V.L. Sveshnikova[a]

[a]*National Research Tomsk State University, 36, Lenin avenue, Tomsk 634050, Russia*

Abstract

The Penchenga Neoproterozoic linear fenite-carbonatite complex in the Yenisei Ridge consists of several magnesiocarbonatite sheet-like bodies which lie nearly concordantly with the metamorphic country rocks and are surrounded with alkaline metasomatic fenite aureoles. Their mineralogy includes primary high-temperature phases (ferrodolomite, calcite, phlogopite, sodic amphibole of the eckermannite – magnesio-arfvedsonite series, fluorapatite, magnetite, and ilmenite), late-magmatic accessories (fluorocalciopyrochlore, pyrrhotite, pyrite, Cu-Pb-Zn-Ag sulfide and hessite, monazite-(Ce) and REE-carbonates of synchysite, cordylite, cebaite, and ancylite), as well as secondary phases (Sr-Ba pyrochlore, ferrocolumbite, fersmite, and Fe and Sr carbonates) of hydrothermal and supergene origin that replace primary magmatic minerals. According to their main features of mineralogy and chemistry, the carbonatites correspond to magnesian derivates of a high-pressure alkali-dolomite melt that forms by melting of carbonated peridotite, as obtained in experiments. The Nd, Sr, and Pb isotope compositions of the Penchenga rocks and minerals ($\varepsilon_{Nd} \approx +6$; $\varepsilon_{Sr} \approx -19$; ~0.81 $^{207}Pb/^{206}Pb$; ~1.99 $^{208}Pb/^{206}Pb$) suggest a mantle PREMA + EM 2 source of carbonatite magma and mineralization (including Nb and REE). The presence of carbonates with relatively high $\delta^{18}O$ and pyrrhotite enriched in $\delta^{34}S$ and ^{207}Pb may be due to continental crust inputs to the source of metals. As estimated approximately from the composition of the pyrrhotite-sphalerite assemblage, sulfide minerals crystallize at a depth of ~30 km in the lower crust, under a pressure of ~8 kbar. Degassing of the juvenile alkali-dolomite melt and its interaction with meteoric waters leads to fenitization and formation of late

magmatic CO_2–H_2O fluids. These "carbohydrothermal" fluids form from salt melts, and increase in H_2O upon cooling from 600 to 200°C. At lower temperatures of 480–240°C, the O–H isotope systems of magmatic minerals undergo inversion and ensuing closure. REE-bearing mineral phases precipitate from REE-carrier fluids.

Keywords: *Neoproterozoic linear Mg-carbonatites, rare-metal and sulfide mineralization, mantle-derived alkali-dolomite melt, late magmatic fluid, crustal contamination, Yenisei Ridge*

1. Introduction

Carbonatites are carbonate-rich igneous rocks that are commonly comagmatic with a variety of alkaline rocks. They may owe their origin to the activity of mantle plumes, which is especially likely in continental rifting settings (Woolley and Kjarsgaard, 2008a, b; Bell and Simonetti, 2010; Ernst and Bell, 2010) where carbonatitic melts segregate by crystal fractionation and/or liquid immiscibility from alkaline magma (Kjarsgaard and Hamilton, 1988; Lee and Wyllie, 1994; Kjarsgaard et al., 1995; Bell et al., 1998; Veksler et al., 1998a, b). In more rare carbonatite-alkaline complexes from accretionary-collisional orogenic belts, the involvement of sublithospheric mantle may be more or less strongly obscured by interactions of magma with crustal material and metasedimentary brines or other fluids (Pokrovskii et al., 1998; Hou et al., 2006; Doroshkevich et al., 2012; Vrublevskii et al., 2012, 2018a, b, 2019a, b; Baatar et al., 2013; Xu et al., 2014, 2019; Chakhmouradian et al., 2015; Vrublevskii, 2015; Çimen et al., 2018).

There is another separate type of carbontatites: so-called "linear carbonatites" found in both cratonic and orogenic settings (Bagdasarov, 1979, 2014; Lapin and Ploshko, 1988; Bulnaev, 2000) worldwide: Chernigov, Dubrava, and Siilinjärvi in the East European Platform; Ilmen–Vishnevogorsk in the Urals; Newania in India; Loe Shilman and Sillai Patti in Pakistan; Qinling orogen carbonatites in China (Puustinen, 1971; Glevasskii and Krivdik, 1981; Mian and Le Bas, 1987; Bocharov and Frolov, 1993; Levin et al., 1997; Viladkar, 1998; Nedosekova et al., 2009; Xu et al., 2014). Some linear carbonatites have no obvious genetic relation with alkaline igneous

rocks but may coexist with fenite, such as the Neoproterozoic Penchenga fenite-carbonatite complex in the Southern Trans-Angara area of the Yenisei Ridge which consists of pyrochlore-bearing magnesiocarbonatites surrounded with alkaline metasomatic aureoles (Zabrodin and Malyshev, 1975; Lapin et al., 1987; Kornev et al., 1999). According to experimental data (Lee and Wyllie, 1998, 2000), mantle carbonatite magma of this type can originate and emplace independently rather than by differentiation of alkaline melt (e.g., Tilton et al., 1998; Vrublevskii et al., 2003; Zozulya et al., 2007; Doroshkevich et al., 2010).

Carbonatites are remarkable in bearing high-temperature apatite-group phosphates and rare-metal (Nb–Ta, REE) and sulfide mineralization (e.g., Kapustin, 1980; Eriksson, 1989; Chakhmouradian and Mitchell, 1998; Viladkar, 1998; Zaitsev et al., 1998a, 2011; Hogarth et al., 2000; Wall and Zaitsev, 2004; Karchevsky, 2005; Chakhmouradian et al., 2017). The mineralization patterns are commonly attributed to changes in the conditions of petrogenesis (Veksler et al., 1998a; Hogarth et al., 2000; Mitchell and Kjarsgaard, 2004; Chakhmouradian and Zaitsev, 2012; Kynicky et al., 2012; Williams-Jones et al., 2012; Martin et al., 2013; Migdisov and Williams-Jones, 2014; Vrublevskii, 2015; Chakhmouradian et al., 2015, 2017; Bataleva et al., 2016b; Feng et al., 2016; Song et al., 2016; Andersen et al., 2017; Bodeving et al., 2017; Tremblay et al., 2017; Smith et al., 2018).

The revealed mineralogy and major- and trace-element compositions of Mg-carbonatites in the Yenisei Ridge are consistent with a model implying high-temperature origin and crystallization from a juvenile mantle alkali-dolomite melt, while fenitization and mineralization result from degassing of the melt and its interaction with meteoric waters which produced late magmatic CO_2-H_2 fluids.

2. Geological background

The major structures of the Yenisei Ridge collisional orogen presumably formed on the margin of the Siberian craton during the Mesoproterozoic (Stenian-Tonian, ~ 1100–850 Ma) and

Neoproterozoic (Cryogenian, 760–720 Ma) events (Vernikovsky et al., 2003, 2009; Likhanov et al., 2014; Kuzmichev and Sklyarov, 2016). In addition to tectonic activity, the area underwent voluminous plutonism (Vernikovsky and Vernikovskaya, 2006) and metamorphism (two events ~850 and 800 Ma ago) (Likhanov et al., 2015). Within-plate magmatism in Transangaria, including intrusion of alkaline and carbonatite magma, was approximately coeval (~730–610 Ma) with rifting (Vrublevskii et al., 2003, 2011; Sazonov et al., 2007; Nozhkin et al., 2008; Vernikovsky et al., 2008; Romanova et al., 2012) and was maintained by a superplume which was responsible for the breakup of Rodinia and acted upon the active margin of the Paleo-Asian Ocean. The products of magmatism occur mainly in the Central Angara terrane along the Tatarka-Ishimba Fault.

The Penchenga linear carbonatite complex is located in the upper reaches of the Bolshaya Penchenga and Tatarka rivers (59°17' N, 94°12' E), tributaries of the Bolshoy Pit and the Angara. It consists of sheet- and lens-like carbonatite bodies surrounded with thick fenite aureoles that form a 25 km long by 2-6 km wide N—S steeply dipping zone along the Tatarka-Ishimba Fault (Fig. 1). They intrude Neoproterozoic marbles, mica schists, and metamorphic mafic rocks. Separate large carbonatite bodies or 120–150 m thick clusters of closely spaced smaller veins are nearly concordant with the country rocks. There are no genetically associated alkaline intrusions in the area.

The mineralogy of carbonatites includes predominant ferrodolomite and calcite (50–90 vol. %), as well as 15–30 vol. % phlogopite and sodic amphibole, 10–15 vol. % apatite, 3–5 vol. % magnetite, and minor pyrrhotite, pyrochlore, and other accessories (Lapin et al., 1987; Vrublevskii et al., 2003). The rocks are comparable with typical magnesiocarbonatites in element contents (Woolley and Kempe, 1989) and show enrichment in P (P_2O_5 to 8–10 wt. %), LREE (to 1200–2000 ppm, La/Yb 80–140), Nb (to 6000–15000 ppm), and Sr (to 4000–9000 ppm). Features of the Nd, Sr, C, O, H, and S isotope compositions indicate a depleted mantle source, crustal contamination, and postmagmatic alteration.

K–Ar and Rb–Sr dating of the Penchenga rocks constrains their emplacement in a range of ≈640–660 Ma (Sobachenko et al., 1986; Lapin et al., 1987). The Sm–Nd isochron ages of amphibole, apatite, and pyrochlore likewise fall within the Late Precambrian: ~672 Ma (Vrublevskii et al., 2003). The most reasonable date (725.9 ± 6.3 Ma) was obtained by Ar–Ar dating of Mg-arfvedsonite (Vrublevskii et al., 2011) and is coeval with alkaline magmatism in the Yenisei Ridge.

3. Analytical methods

Mineral chemistry was studied by the electron microprobe analysis on a *Tescan Vega II LMU* scanning electron microscope with an Oxford *INCA Energy 350* EDS system operated at an accelerating voltage of 20 kV, a beam current of 5 nA, a beam size of 1–2 μm, and 120 s count time. The operation conditions were the same for all minerals. The results were checked against natural minerals and synthetic phases used as standards (MAC 55 Standard Universal Block Layout+F/Cup, Micro-Analysis Consultants Ltd, UK) for calibration. The analyses were carried out at the National Research Tomsk State University (Tomsk).

The X-ray diffraction (XRD) analysis for identification of crystal structure in pyrochlore and pyrrhotite was applied to powder aliquots on a PANalytical *X'Pert PRO* diffractometer at the National Research Tomsk State University (Tomsk). The scanning was performed using a CuK_{α} anode tube, at an accelerating voltage of 40 kV and a beam current of 30 mA, at the angles 2Θ 4 to 60° with a stepsize of 0.02°, a rate of 30 revolutions per minute, and a count time of 0.1 s per step. The spectra were interpreted using the *HighScore* software, with reference to PDF-4 (Powder Diffraction File 2014).

The gas phase composition of solid carbonate and fluid microinclusions in apatite was determined on a gas chromatography analyzer following a method (Osorgin, 1990) designed at the Laboratory of Thermobarogeochemistry of the Institute of Geology and Mineralogy (Novosibirsk). Inclusions were heated in vacuum; helium was used as a carrier gas (20–60

cm^3/min); hydrogen and air were supplied, at rates of 20 and 200 cm^3/min, to two flame-ionization detectors, respectively.

The Pb isotope composition of pyrrhotite from the Penchenga samples was measured by the standard techniques on a Thermo Scientific *Neptune MC-ICP-MS* mass spectrometer (Germany) at the Institute of Geology of Mineral Deposits, Petrography, Mineralogy and Geochemistry (Moscow) using the approach detailed by Chernyshev et al. (2007). Lead for mass spectrometry was extracted from 10 to 15 mg aliquots digested in a mixture of HCl+HNO_3 in an HBr medium, on chromatographic columns with 1×8 Bio-Rad AG anionite. The total procedural Pb blank controlled by isotopic dilution did not exceed 0.1 ng. Before isotope analysis, the Pb solutions (3% HNO_3) were pre-traced by Tl with a known $^{205}Tl/^{203}Tl$ ratio. The sample solution was introduced into the mass-spectrometer torch using a quartz spray chamber (wet plasma mode). All measured Pb isotope ratios were normalized to the standard $^{205}Tl/^{203}Tl$ ratio of 2.3889 ± 2. The analytical precision and accuracy were evaluated from the results for the USGS standard samples of AGV-2 ($^{206}Pb/^{204}Pb$=18.871 ± 5; $^{207}Pb/^{204}Pb$=15.621 ± 4; $^{208}Pb/^{204}Pb$=38.548 ± 10) (n=5) and BCR-1 ($^{206}Pb/^{204}Pb$=18.822 ± 6; $^{207}Pb/^{204}Pb$=15.640 ± 4; $^{208}Pb/^{204}Pb$=38.737 ± 12) (n=10). The total error (±2σ) of Pb analysis was within ± 0.04%.

The results of the study are discussed with reference to our earlier data on average major and trace element contents (XRF, ICP-MS) and isotope geochemistry (stable C, O, H, S and radiogenic Nd, Sr isotopes) for carbonatites and fenites (Vrublevskii et al., 2003).

4. Petrography and mineral chemistry of magnesiocarbonatites

4.1. Structure, texture and main mineralogy

The Penchenga Mg-carbonatites are massive or have pegmatitic or trachytoidal textures, often with banded or lens-like distribution of rock-forming minerals (Figs. 2, 3a, c–d). The heterogeneity may be evidence of their magmatic origin and turbulent intrusion of a highly mobile melt. On the other hand, the rocks lack signatures of pseudomorphism after primary

phlogopite or magnetite, which are common to later fluid dolomitization (Chakhmouradian et al., 2016). The rims of some coarse ferrodolomite grains are cataclased (Fig. 2c), possibly, by dynamic metamorphism in a regional fault.

Pegmatitic varieties are mainly (≥ 90 %) composed of inequigranular carbonates with minor percentages of phlogopite, apatite, pyrrhotite, and pyrochlore. They are less abundant than rather melanocratic trachitoidal rocks with linearly oriented crystals of alkali-amphibole and mica set in a fine- and medium-grained mosaic carbonate aggregate (Fig. 3c–f). The trachytoidal varieties contain different percentages of apatite, magnetite, sulfides, and pyrochlore which make up to 40–50 vol. %, together with femic silicates.

4.2. Rock-forming minerals

Carbonates. Ferrodolomite is the most widespread carbonate phase. It contains around 31–33 wt. % CaO, 17–21 wt. % MgO, 5–10 wt. % FeOt, 0.9–2.2 wt. % MnO (Table. 1), and commonly within 1 wt. % SrO. The concentrations of MgO, FeO(t), MnO and SrO in paragenetic calcite, at stoichiometric CaO (54–55 wt. %), are within ~1–2 wt. %. Late during carbonatite formation, primary carbonates become replaced by ankerite and siderite with up to 27–63 wt. % FeO(t) and 1–13 wt. % MgO.

Fe-Mg silicates form the primary paragenesis of phlogopite and alkali amphiboles and are among major constituents of the fenite-carbonatite assemblage (Fig. 2a–d). Phlogopite contains as high as 20–24 wt. % MgO (0.7–0.9 Mg# at ~3–13 wt. % FeOt) and up to 10–11 wt. % K_2O, and has relatively high Mg/Fe^{2+} ratios (2.7–13.7) due to isomorphism in the phlogopite–annite join (Table 2; Fig. 4a). Mica varieties from schlieren at the intrusion margins have notably lower Mg contents (12–15 wt. % MgO; 16–20 wt. % FeOt; Mg# = 0.5–0.6, Mg/Fe^{2+} = 1.1–1.7) and up to 2 wt. % TiO_2. Similar relative contents of Mg and Fe are common to biotite from fenites with higher TiO_2 of 3–6 wt. % (Table 3). Phlogopite has an almost stoichiometric number of Si and Al cations (around 3.00–3.12 (41–42 wt. % SiO_2) and 1.00–1.05 (11–12 wt. % Al_2O_3), respectively) and is

comparable with that from mantle dolomite carbonatite (Fig. 4b). The composition difference of biotite results from the respective variations in SiO_2 and Al_2O_3 (about 37–40 and 11–16 wt. %, respectively).

Amphiboles are rather sodic low-Ti (Na_2O 7.5–9.7; TiO_2 < 0.4 wt. %) varieties of the eckermannite-magnesioarfvedsonite join (Table 4; Fig. 5a, b) with low CaO (0.6–3 wt. %) and Al_2O_3 (0.3–2 wt. %) and high magnesian contents (~15–20 wt. % MgO; Mg# = 0.7–0.8), which is common to many magmatic carbonatites (Samoilov and Gormasheva, 1975; Le Bas and Srivastava, 1989). Fenites and schlieren along the margins bear also Mg-riebeckite with ~7 wt.% Na_2O (Table 3). As in the case of melanocratic micas, distinct correlation between Mg and Fe cations indicates chemical parentage of the analyzed amphiboles which apparently belong to the same join (Fig. 5c, d).

Apatite occurs as colorless short-prismatic cracked and abraded crystals which are uniformly distributed over the rock volume or make band-like patterns (Figs. 2h, 3c–f). The contents of major elements are little variable, with 52.2–53 wt. % CaO, 41.6–41.8 wt. % P_2O_5, and 3.1–3.4 wt. % F (Table 5) and comparable with those in carbonatitic fluorapatite (e.g., Le Bas and Handley, 1979; Hogarth, 1989; Bühn et al., 2001); SrO and REE are within 2.6 and 1 wt. %, respectively, which is typical of apatite crystallized from high-temperature carbonatite magma (Kapustin, 1980).

The *ilmenite-magnetite assemblage* is of a limited occurrence in the analyzed carbonatite samples. Predominant magnetite occurs as isolated octahedral crystals, sometimes up to 5–10 cm, or as small polycrystalline aggregates resorbed by residual carbonate melt. Magnetite segregations enclose small apatite and amphibole grains and bear signatures of exsolution in some cases (Fig. 6c, d). Magnetites have little variable element contents, with ~92.4–93.4 wt. % FeO(t) and 0.35–0.52 wt. % TiO_2 (Table 6).

There are two generations of ilmenite: thin exsolution lamelli or later irregularly shaped segregations that replace magnetite along cracks and on the crystal periphery, while the

coexisting apatite and amphibole grains are resorbed and broken into dispersed fragments (Fig. 6e, f). Ilmenite is comparable with its typomorphic varieties from alkaline-carbonatite complexes (Chernyshova, 1989) in TiO_2/FeO(t) ratios of ~1.2–1.3 with 52–53 wt. % TiO_2 and 40–44 wt. % FeO(t) (Table 6), elevated MnO (2.9–4.9 wt. %), and intermediate percentages of the geikielite component (MgO ~1.2 wt. %). Ilmenorutile from fenite has a high Nb enrichment with 6.3 wt. % Nb_2O_5; 89 wt. % TiO_2, 3.2 wt. % FeO(t), and 0.9 wt. % MgO (Lapin et al., 1987), which is quite frequent in carbonatites.

4.3. Ta-Nb mineralization

The concentrations of Nb and Ta in Mg-carbonatites are controlled by the distribution of pyrochlore, ferrocolumbite, and fersmite. Pyrochlore commonly occurs as dispersed fine yellowish-brown euhedral grains (Fig. 7f–g) of mainly octahedral habits with reduced cubic and rhombic-dodecahedral faces, or sometimes as isolated coarse crystals or intergrowths reaching sizes of 10–15 cm (Fig. 7a–f). The crystal surfaces are either smooth or stepped, the latter possibly being due to uneven material inputs to the nucleation centers. While growing, pyrochlore can capture small syngenetic segregations of sodic amphibole and apatite but then becomes resorbed by carbonate melt, which leads to the formation of skeletal crystals (Figs. 6a, b; 7h, i). Sr-Ba pyrochlore varieties, as well as ferrocolumbite and fersmite, likely formed later, after primary magmatic pyrochlore.

Pyrochlore in trachytoidal and pegmatitic carbonatites is of two generations (I and II) (Table 7). Both lack U, Th, Fe and REE and have quite low Ta_2O_5 contents (0.8–3.1 wt. %). The contents of other major oxides (14–15 wt. % CaO, 6.2–8.1 wt. % Na_2O, 67–72 wt. % Nb_2O_5, and 0.6–0.9 wt. % TiO_2) actually correspond to the stoichiometry (Nb + Ta > 2Ti and Nb > Ta (Kostov, 1968; Hogarth, 1977). Pyrochlore II contains slightly less Nb and has a slightly higher Ta_2O_5/Nb_2O_5 ratio (0.04–0.05), which is typical of primary U-free pyrochlore of linear carbonatite complexes (Chernyshova, 1989). Taking into account the presence of fluorine (≈5 wt. %), both mineral

varieties can be classified as fluorocalciopyrochlore (Atencio et al., 2010). Ca and Na are major cations and occupy all *A* sites in the structure (0.9–1.0 apfu Ca and 0.73–0.98 apfu Na; Na/Ca ~0.8–1). The V(*A*) vacancies are commonly within 0.03–0.4 apfu (Fig. 8), as in magmatic pyrochlore (Nasraoui and Bilal, 2000).

The crystals of pyrochlore I and II include small (n × 100 μm) sites of later Nb-bearing minerals among which Sr–Ba pyrochlore (pyrochlore III), ferrocolumbite and fersmite. Pyrochlore III contains much less Nb_2O_5 (52.4–61.5 wt. %) but more Ta_2O_5 (~ 4–17 wt. %, with Ta_2O_5/Nb_2O_5 = 0.06–0.34) than the primary varieties. Strontium and barium substitute for almost all Na and a half of Ca cations (Na/Ca ~ 0.1–0.3) at the *A* sites: 5.1–7.6 wt. % or 0.20–0.28 apfu SrO and 4.3–8.3 wt. % or 0.10–0.23 apfu BaO. The F content in the mineral is vanishing while FeO(t) and SiO_2 are higher (to 2–3 wt. %), and the V(*A*) vacancies reach 0.8–1.1 apfu, commonly as a result of hydrothermal or supergene alteration of pyrochlore (Lapin and Kulikova, 1989; Wall et al., 1996). This may be the reason why some samples contain uranium (2.9 wt. % UO_2), thorium (≈ 1 wt. % ThO_2, according to Popova et al., 2017), and titanium (1.7 wt. % TiO_2). Weathered carbonatites likewise store Sr and Ba pyrochlore with up to 72–73 wt.% Nb_2O_5 and 1 wt. % Ce_2O_3, and have V(*A*) vacancies of 1.2–1.4 apfu (Table 7).

The XRD analysis of pyrochlore from fresh and weathered carbonatites shows similar unit cell sizes (a_0 = 10.434–10.444 Å) corresponding to the standard crystalline pyrochlore. Its typical peaks, of similar intensity and *d*-spacing, appear in the XRD profiles obtained at the 2Θ angles from 14 to 50° (Fig. 9; Table 8). The presence of additional low peaks in the 24–35° 2Θ region is evidence of a microlite component, according to the PDF-4 analytical database.

Ferrocolumbite and *fersmite* replace primary pyrochlore, presumably by the hydrothermal effect (nos. 1–3 in Table 9). The two minerals are rich in Nb_2O_5 (~77–79 wt. %), with Ta_2O_5/Nb_2O_5 ~ 0.02–0.06. Ferrocolumbite contains 15.5 wt. % FeO(t), 1.7–2.2 wt. % MgO, and 1.5–1.9 wt. % MnO. Fersmite typically has 16 wt. % CaO and 1.74 wt. % Ce_2O_3. The contents of FeO(t) in ferrocolumbite from the zone of supergene alteration reach 19–20 wt. %.

4.4. Sulfide mineralization

Sulfide mineralization in Mg-carbonatites shows no species diversity. The most widespread pyrrhotite is uniformly disseminated or forms massive vein zones (Fig. 2h). Pyrrhotite grains enclose particles of rock-forming silicates, carbonates and apatite, as well as small crystalline ingrowths, nests, and filaments of pyrite, chalcopyrite, sphalerite, and galena, and microinclusions of Ag-bearing sulfides (argentite and argentopentlandite) and tellurides (hessite) (Fig. 6; Tables 10, 11).

Pyrrhotite and *pyrite.* Atomic percentages of iron and sulfur in pyrrhotite vary slightly: 46.9 to 47.2 at. % and 53.1 to 52.8 at. %, respectively, and are comparable with Fe/S ratios in hexagonal (~0.90) and monoclinic (~0.87) varieties of the mineral (Fig. 10). The variations may result from cooling and/or redox changes in the growth medium. Pyrrhotite has similar features in HT phoscorite and carbonatite of the Kola alkaline province (Kovdor and Khibiny plutons) and South Africa (Palabora pluton) (Rudashevsky et al., 1995; Bulakh et al., 1998; Zaitsev et al., 1998a). The XRD spectra of the analyzed pyrrhotites contain hkl peaks (102) with a *d*-spacing of $d \approx 2.06$ Å in the range 2Θ 43.5–44.5°, of the same shape and intensity (Fig. 9; Table 8), which confirms the hexagonal symmetry.

Later stoichiometric pyrite (S/Fe 1.94–1.98) commonly grows together with pyrrhotite and resorbes the latter and the host ferrodolomite. Skeletal pyrite crystals sometimes occur along cracks in carbonate and amphibole, which is evidence of rapid growth in a viscous medium (Fig. 6h–k). Postcrystallization reactions of pyrrhotite and pyrite produced rims and vein aggregates of goethite and barite (Fig. 6k, m). Oxidation of sulfides and the formation of sulfate sulfur are caused by activity of oxygen as the growth medium increases in Eh (Karchevsky, 2005).

Cu-Pb-Zn sulfides. Chalcopyrite (around 34–35 wt. % Cu, 30 wt. % Fe, and 34–35 wt. % S) exists as anhedral inclusions and thin veinlets in pyrrhotite and does not deviate from the theoretical composition. It coexists with scarce irregular segregations of sphalerite and galena

(Fig. 6g, l, n; Table 10). Sphalerite lacks Cu and contains up to ~7–8 wt. % Fe (~12–14 mole % FeS), which corresponds to the conditions of the sphalerite-pyrrhotite geobarometer (P, kb = 42.30 – 32.10 log mole % FeS; Hutchison and Scott, 1981). According to approximate estimates on this basis, the sulfide minerals formed under a pressure of ~5.4–7.6 kbar at a depth of ~18–25 km. Fe-sphalerite shows slightly unusual concentrations of Cd as high as 0.5–1.9 wt. %. Apatite encloses an in-grown galena crystal of a different stoichiometry (~82 wt. % Pb, 13.5 wt. % S), with ~4 wt. % Fe.

Ag-bearing minerals (Table 11) are sulfides (argentite and argentopentlandite) and telluride (hessite), which are very rare in the analyzed carbonatites. They occur as fine (within 10–15 μm) mineral inclusions in pyrrhotite or in dolomite, apatite, and chalcopyrite at the boundary with pyrrhotite. Argentite contains ~83 wt. % Ag, 11.6 wt. % S, and minor Fe and Cu (3.7 and 1.6 wt. %, respectively). The concentrations of Ag in hessite (~61 wt. % at 37.5 wt. % Te) and argentopentlandite (~10–13 wt. %) generally agree with those in the respective phases from the Kovdor carbonatite (Rudashevsky et al., 1995). The ranges of Fe, Ni and S in argentopentlandite are typically 33–40 wt. %, 13–21 wt. %, and 30.7–32.8 wt. %, respectively.

4.5. REE mineralization

Most of LREE and Sr in the Penchenga carbonatites reside in disseminated monazite, as well as in Ca- and Ba-bearing REE-fluorocarbonates, Sr-REE carbonates, and strontianite formed after primary ferrodolomite and calcite. Most segregations are within 10–50 μm in size and are localized along the grain boundaries of pyrrhotite, apatite and rock-forming carbonates. Disseminated fluorocarbonates in apatite and calcite, as well as in Sr-REE from siderite veinlets, are of more limited occurrence.

Monazite is a Ce-rich variety (monazite-(Ce)), with ~35 wt. % Ce_2O_3, 17–24 wt. % La_2O_3, 2.1–2.5 wt. % Pr_2O_3, and ~67–69 wt. % ΣLn_2O_3(La+Ce+Pr+Nd) (Table 5). It exists as two generations with different La/Ce and La/Nd ratios: ~0.5 or 0.7 and ~1.4 or 3.1, respectively (at Nd_2O_3 7.6–

12.3 wt. %). The coexisting REE carbonates have much lower concentrations of lanthanides (~32–53 wt. % ΣLn_2O_3; Fig. 11a, b). This heterogeneity of monazite, including in carbonatites, may result from dissolution of earlier REE-bearing phases or from changes in the chemical activity of REE in melts and fluids (e.g., Förster, 1998; Zhu and O'Nions, 1999). We found small segregations of monazite (≈ 61 wt. % ΣLn_2O_3(La+Ce+Nd)) and xenotime (37.8 wt. % Y_2O_3; 15.5 wt. % ΣLn_2O_3(Gd+Dy+Er+Yb)) in the Penchenga fenite, which were possibly produced by degassing of carbonatite magma.

Ca-REE fluorocarbonate is synchysite-(Ce) with 14.9–16.3 wt. % CaO, ≈ 53 wt. % ΣLn_2O_3, at La/Ce = 0.7 and La/Nd = 2.9–3.3 (Table 12), and <1–2 wt. % SrO and BaO. It commonly occurs as two generations of fine acicular or anhedral crystals intergrown with calcite, ferrodolomite, and ancylite (Fig. 6 p, q). Compositionally similar synchysite is known from late magmatic carbonatites in the Wicheeda complex (Canada) and in the Khibiny alkaline intrusion (Dalsin et al., 2015; Zaitsev et al., 1998b).

Ba-REE fluorocarbonates (Table 13) are restricted to sporadic anhedral grains and are Ce varieties of cordylite and cebaite according to EMPA. The major-element composition of cordylite-(Ce) with 23.7–26.4 wt. % BaO, 1.9–3.0 wt. % Na_2O, 4.25–4.59 wt. % CaO, 4.37–6.27 wt. % SrO, and 35.3–39.9 ΣLn_2O_3 corresponds to the formula $(Na_{0.55}Ca_{0.51})_{1.06}Ba_{1.07}(Ce_{0.77}La_{0.56}Nd_{0.17}Sr_{0.34})_{1.84}(CO_3)_{4.00}F_{0.87}$ and is similar to that of Ca- and Sr-rich cordylite from the Khibiny carbonatites (Zaitsev et al., 1998b). Cebaite-(Ce) exists as very small (n × 1 μm) scarce grains and is similar to its counterparts from other carbonatite complexes in the contents of BaO (~41.0 wt. %) and ΣLn_2O_3 (~32.4 wt. %), but contains almost twice higher Sr and Ca, which makes its composition consistent with the theoretical formula. Cordylite and cebaite have much higher La/Ce (0.8–0.9) and La/Nd to (4–5) ratios than the coexisting monazite and other REE carbonates.

Sr-carbonates are ancylite-(Ce) and strontianite which occur as small segregations, mainly in calcite (Fig. 6o). Ancylite has a variable composition with 17.5–21.8 wt. % SrO, 43.9–52.2 wt. %

ΣLn_2O_3, and 2.1–3.6 wt. % CaO, which is known also from other occurrences (Table 12). The coexisting strontianite likewise shows variations of SrO (~61–69 wt. %) and CaO (~3–10 wt. %) (Table 1) discordant with the stoichiometry of pure $SrCO_3$, probably, as a result of isomorphic substitutions.

5. Discussion

5.1. Sources of Mg-carbonatite magma

The formation of linear carbonatite complexes of any age and petrography is often attributed to the evolution of mantle magmatism (e.g., Zozulya et al., 2007; Nedosekova et al., 2009, 2013; Doroshkevich et al., 2010) derived from depleted, enriched, or mixed sources, possibly, with a plume contribution, as indicated by trace-element compositions and radiogenic isotopes (Nedosekova et al., 2009).

Isotope geochronology places the origin of the Penchenga fenite-carbonatite complex at ~725 Ma (Vrublevskii et al., 2011), i.e., about the time of Neoproterozoic rifting in the Rodinia supercontinent. Rifting and related magmatism likely resulted from the activity of a large mantle plume (Nozhkin et al., 2008). The primary ratios of $^{143}Nd/^{144}Nd_{725}$ (0.51200–0.51203, $\varepsilon_{Nd}(t)$ 5.8–6.3) and $^{87}Sr/^{86}Sr_{725}$ (0.70228–0.70233, $\varepsilon_{Sr}(t) \approx -19$) in the analyzed rocks and minerals (Table 14) indicate possible participation of PREMA-type moderately depleted material in the generation of juvenile carbonatite melt. Similar values ($\varepsilon_{Nd}(t)$ = 4–6 and $^{87}Sr/^{86}Sr(t)$ = 0.7025–0.7033) are observed in late Neoproterozoic (Riphean-Vendian) alkaline and subalkaline intrusions from the Yenisei Ridge (Fig. 12a). Carbonatites from other linear complexes of different ages and tectonic settings worldwide (Ural Mountains, Karelian Craton, Indus Suture Zone in the NW Pakistan) likewise fall within the domain of mantle components. There are signatures of enriched (EM) and depleted juvenile mantle mixing at the magma source, which is common to carbonatite magmatism (Bell and Tilton, 2001). The presence of depleted mantle material in the parent magma may be responsible for the Nd–Sr signatures observed in

Mesoproterozoic–Neoproterozoic and Paleozoic (Devonian) carbonatites of the Superior alkaline province, Canadian shield ($\varepsilon_{Nd}(t) \sim 1–5$; $\varepsilon_{Sr}(t) \sim$ from –12 to –4) and of the Kola alkaline province, Baltic shield ($\varepsilon_{Nd}(t) \sim 2–7$; $\varepsilon_{Sr}(t) \sim$ from –15 to 0), respectively (Bell and Blenkinsop, 1989; Kramm, 1993; Kramm and Kogarko, 1994; Lee et al., 2006; Wu et al., 2017), as well as in Late Permian carbonatites of the Tarim Block, NW China ($\varepsilon_{Nd}(t) \sim 1–4$; $^{87}Sr/^{86}Sr(t)$ 0.7037–0.7041; after Song et al., 2017).

The lead isotope composition ($^{207}Pb/^{206}Pb_{725}$ 0.812, $^{208}Pb/^{206}Pb_{725}$ 1.999) in pyrrhotite from the Penchenga carbonatites indicate EM2 involvement into magma generation (Table 15; Fig. 12c, d). The mineral chemistry of pyrrhotite slightly departs from the general Pb-isotope trend for Mesozoic-Cenozoic nephelinite-carbonatite volcanoes of East Africa fed from a source of mixed depleted and enriched mantle components (Bell and Tilton, 2001). The observed ^{207}Pb and ^{206}Pb enrichments of pyrrhotite are consistent with a contribution of upper crustal material, like the case of Paleozoic alkaline and carbonatite complexes in the Kuznetsk Alatau and Gorny Altai areas in the western Central Asian Orogenic Belt (Fig. 12b). On the other hand, the variable Pb isotopic ratios of galena from alkaline-ultramafic carbonatites in the Baltic shield (Kovdor, Sallanlatvi, Sebljavr, Vuohijärvi), with averages of $^{206}Pb/^{204}Pb = 18.42$, $^{207}Pb/^{204}Pb = 15.58$, and $^{208}Pb/^{204}Pb = 38.30$, were attributed to isotopic differences preserved within a sublithospheric mantle source (Bell et al., 2015).

The carbon and oxygen isotope compositions in the rock-forming ferrodolomite of the Penchenga complex likewise indicate possible contamination of the carbonatite melt with upper crustal material (Fig. 13a; Table 16). The predominant compositions of $\delta^{13}C_{PDB}$ from –6 to –4 ‰ and $\delta^{18}O_{SMOW}$ ~8–11 ‰ fall within the ranges for primary carbonatites or show direct correlation that results from high-temperature (~700–800˚C) isotope fractionation of a cooling carbonated melt (Deines, 1989; Ray et al., 2010). However, the relatively high $\delta^{18}O$ values rather indicate inputs of crustal material and mixing of mantle and crustal CO_2. Similar signatures are more or less prominent in the Siilinjärvi and Newania linear carbonatite complexes

(Thichomirowa et al., 2006; Viladkar, 1998; Ray et al., 2010), as well as in carbonatites from the area of the South Qinling orogeny and the Foreland belt, Canadian Cordillera, which lack any genetic relation with alkaline igneous rocks (Xu et al., 2014; Trofanenko et al., 2016) (see Fig 13a). This interaction may be possible upon recycling/decompressional melting of sedimentary material in subcontinental mantle (Song et al., 2017), which may result from deep slab subduction as an essential agent in post-collisional alkaline or carbonatite magmatism, in Phanerozoic or even Precambrian settings (Xue et al., 2018; Xu et al., 2019).

5.2. Conditions of magnesiocarbonatite petrogenesis

The mantle origin of linear carbonatites has no explicit implications for the mechanisms and conditions of their petrogenesis, which has been explained in terms of magmatism or metasomatism (e.g., Samoilov, 1984; Bulnaev, 2000; Bagdasarov, 2014). Judging by their mineralogy and chemistry, the Penchenga carbonatites may have crystallized from a juvenile alkaline-dolomite melt. The assemblage of earliest crystallized minerals includes high-temperature Fe–Mg silicates, apatite, and magnetite. Note that magnesioarfvedsonite predominant among amphiboles has Mg# up to 0.8 and low Al_2O_3 and TiO_2 contents (Table 4), which is evidence of equilibrium with Mg-carbonatite melt and related phlogopite (Samoilov and Gormasheva, 1975; Le Bas and Srivastava, 1989). Co-crystallization of magnesioriebeckite and biotite in fenite may be evidence of lower temperatures. The direct correlation of Mg and Fe cations observed in silicates confirms their genetic relationship (Fig. 4c, d). The primary banding of rocks, abrasion signatures in apatite crystals, and magnetite-ilmenite exsolution lamelli (T < 600°C), as well as the presence of hexagonal pyrrhotite, indicate that the carbonatites formed at high temperatures in the presence of salt melts. The paragenetic relation of pyrrhotite with Fe-sphalerite (geobarometry, after Hutchison and Scott, 1981) suggests crystallization in the lower crust (~18–25 km and ~5.4–7.6 kb).

The number of vacancies in the primary pyrochlore formula (V*A* = 0.03–0.4 apfu; Fig. 8b), as well as the atomic percentages of Ca, Na and V*A* vacancies in pyrochlore I and II, agree with those of primary niobates in magmatic carbonatites (Nasraoui and Bilal, 2000; Zurevinski and Mitchell, 2004; Chakhmouradian et al., 2015). Newly formed Sr-Ba-pyrochlore has more vacancies (0.8 to 1.4 apfu V*A*) and shows a secondary trend, because Sr and Ba substitution for Na and Ca fails to keep up with their increasing deficit caused by hydrothermal and supergene leaching. Pyrochlore-group minerals from a similar linear carbonatite complex of Newania in India illustrate how low-temperature hydrothermal alteration can obscure the magmatic origin of carbonatite. On the other hand, pyrochlore in the Penchenga rocks shows low Ta/Nb ratios within 1/40 to 1/150 commensurate with those (<1/70) in magmatic carbonatite (Möller, 1989).

The principal possibility for generation of alkaline-dolomite magma by low-degree melting of carbonated mantle peridotite at 2–7 GPa was proven in experiments (e.g., Wallace and Green, 1988; Wyllie and Lee, 1998; Lee and Wyllie, 2000). Even small batches of this magma, along with a mantle plume, can rise from depths at least 70 km, and then become degassed and crystallize as magnesiocarbonatite. The major-element compositions of the Penchenga rocks correspond to Mg- carbonatites and are very similar to experimental dolomite melts (Fig. 14). Most compositions lie at the boundary between the liquidus fields of vapor-saturated carbonates and silicates, where their position is controlled by the equilibrium of carbonated melt (dolomite + Mg-calcite) with main mineral phases of mantle lherzolite (at *Q* = 1230˚C, 2.8 GPa).

We observed signatures of such a melt in the Penchenga carbonatites as round monocrystalline carbonate microinclusions entrapped by growing apatite (≤ 50–100 μm). For comparison, Mg-calcite globules in carbonatites from East Africa melted at ≈ 700–900°C after the decrepitation of CO_2–H_2O fluid microinclusions at lower temperatures of 320–590°C (Ting et al., 1994). This change in the mineral growth medium is consistent with results of gas chromatography of microinclusions in the Penchenga carbonatites. Apatite apparently nucleated

after the melt entrapment, while the saturated fluid was cooling and CO_2 was decreasing. At the temperatures from 600°C to 200°C, salt melts transform into so-called "carbohydrothermal" fluids consisting mostly of H_2O and CO_2, low CO, and vanishing methane, nitrogen, and molecular hydrogen (Table 17; Fig. 15). It is only at the high-temperature stage of separation that the fluid phase contains the highest total CO_2 + CO (870–1070 ppm), at very low H_2O (~10–70 ppm). Cooling to 500–400°C leads to abrupt decrease in CO_2 and other components. Most of ferrodolomite likely precipitate within this temperature interval. Commensurate temperatures (~ 300–600°C) can be also inferred from decrepitation of fluid microinclusions in apatite from calcite carbonatites of the Kuznetsk Alatau alkaline-mafic intrusion (Vrublevskii et al., 1989; Vrublevskii, 2015).

According to the available models, carbonated melts can be saturated with alkalis, water, and fluorine (e.g., Wallace and Green, 1988; Kjarsgaard et al., 1995; Lee and Wyllie, 1998; Mitchell and Kjarsgaard, 2011). Degassing of alkaline-dolomite magma during the formation of the Penchenga complex may have maintained large-scale fenitization of the country rocks. The ensuing late-magmatic processes, which became more active due to circulation of meteoric waters in the fault zone, led to the formation of a carbohydrothermal fluid. Its effect upset the oxygen and hydrogen isotope systems in minerals but failed to change the mantle tracers in the less sensitive Rb-Sr and Sm-Nd systems of rocks. The isotope disequilibration is responsible for large ranges of $\delta^{18}O$ and δD (from 3.1 to 7.1 ‰ and –154 to –30 ‰, respectively) in coexisting amphiboles and micas in the carbonatites (Table 16). Deuterium and ^{18}O depletion of minerals relative to magmatic fluids appears to result from degassing of the carbonated melt and subsequent mixing of the fluid with hot meteoric waters having negative $\delta^{18}O$ values (Vrublevskii et al., 2003). These processes may be responsible for the formation of fenite aureoles, as well as for the preservation of the $\delta^{18}O$ system of phlogopite, apatite, magnetite, and pyrochlore at lower temperatures (250–480°C). The accessory magnetite and pyrochlore have much lower $\delta^{18}O$ within –0.3 to –3.2 ‰ (Table 16) than the fresh varieties (Conway and Taylor,

1969). Commensurate $\delta^{18}O$ values were reported for minerals from rare-metal carbonatites of the Tomtor complex in Yakutia which recrystallized in similar conditions at ~ 200–300°C (Pokrovskii, 2000).

5.3. Origin of mineralization

The magnesiocarbonatites of the Yenisei Ridge, like many other similar rocks, bear accessory mineralization of three main types: (i) niobium oxides, (ii) sulfides, and (iii) REE carbonates and monazite. The diversity and general paragenetic sequence of minerals formed in the course of the multi-stage history of the carbonatites (Fig. 16).

According to experimental data, pyrochlore is a relatively high-temperature (~930°C) liquidus phase in the system $CaCO_3$–CaF_2–$NaNbO_3$, and its early precipitation in nature may be controlled by differentiation of haplocarbonatite liquids (Mitchell and Kjarsgaard, 2004). The content of $NaNbO_3$ in a synthetic analog of the mineral becomes nearly 2.5 times higher as the temperature decreases to 600°C, at 0.1 GPa. Enrichment of Nb over Ta is especially prominent in systems with high F/OH ratios in the carbonatite melt (Kjarsgaard and Mitchell, 2008). Euhedral pyrochlore grains in the carbonatites we studied are low-Ta (≤ 2–3 wt. % Ta_2O_5) but contain small crystalline inclusions of sodic amphibole and apatite entrapped during the mineral growth. The presence of syngenetic magnetite with exsolution signatures (Fig. 6a–d) suggests that primary pyrochlore I and II formed at a high temperature (at least 600°C) and received Nb from a juvenile source. Niobate, apatite, magnetite, and baddeleyite can crystallize together from a melt, as proven by the example of the Aley calcite-dolomite carbonatite (Canada) of a similar composition (Chakhmouradian et al., 2015). Niobium can be carried by phosphate and F-bearing anion complexes (Hogarth et al., 2000), which leads to co-precipitation of fluorocalciopyrochlore and apatite at the early stage of magmatism. The presence of >1 wt. % F in the melt decreases its crystallization temperature and favors preferable formation of pyrochlore among niobates (Jago and Gittins, 1993; Mitchell and Kjarsgaard, 2004). In the Penchenga carbonatites, ferrocolumbite

and fersmite replace magmatic fluorocalciopyrochlore, which often results from interaction with low-temperature aqueous fluids (Chakhmouradian et al., 2015; Tremblay et al., 2017). In this case, the fluid effect shows up as low $\delta^{18}O$ in coexisting pyrochlore and magnetite. On the other hand, the initial Nd isotope ratio in the analyzed pyrochlore ($\varepsilon_{Nd}(t) \approx 6.2$, see Table 14) prompts a deep source of mineralization. Similar isotopic signatures ($\varepsilon_{Nd}(t)$ up to ~4–5) were reported for calciopyrochlore from soevite of the Paleozoic Ilmenogorsk–Vishnevogorsk linear carbonatite–miaskite complex located in the Ural fold belt. Its igneous derivatives may come from a single magma source in moderately depleted mantle (Nedosekova et al., 2018).

Experiments simulating the interaction of reduced sulfur-bearing fluids with mantle silicates at P = 6.3 GPa and T = 1050–1550°C demonstrate that sulfides and sulfide melts can form at large depths in subduction zones (Bataleva et al., 2016a). Widespread Fe-Mg-Ca carbonates can reach these depths, together with sulfates and pyrite, and participate in the formation of immiscible carbonate and sulfide liquids at $T \geq 1350$°C (Bataleva et al., 2016b). Immiscibility signatures are prominent in ankerite-pyrite and ankerite-olivine-pyrite synthetic systems where newly formed pyrrhotite coexists with dolomite. Paragenetic hexagonal pyrrhotite and Fe-rich sphalerite in the Penchenga carbonatites record a pressure of ~8 km and a depth of ~ 30 km where mantle carbonatite magma can interact with slab sedimentary material. This possibility is supported by the S isotope composition of pyrrhotite (Fig. 13b) which is above the average for carbonatitic sulfides and above the meteorite standard: –0.8 to +9.2 ‰ against –3 to 0 ‰ $\delta^{34}S$ (Deines, 1989). The mixing degree of slab-derived and mantle sulfur apparently depends on the lithology of slab sediments and their contribution to the melt.

The Penchenga magnesiocarbonatites, with average REE contents of ≈790–1770 ppm and LREE enrichment over HREE (LREE/HREE ≈ 15–17; La/Dy_{cn} = 12.4–14.6), are comparable with the respective rocks of magmatic origin (Fig. 17a, c; Table 18). Some other characteristic trace elements likewise reach levels typical of Mg-carbonatite average (Fig. 17b). REE enrichment of carbonatites is known from both model and natural systems (e.g. Veksler et al., 1998a;

Vrublevskii et al., 2012, 2018a; Martin et al., 2013; Vrublevskii, 2015; Bodeving et al., 2017). However, REE in the Penchenga rocks are vanishing (about 1 wt. % Ln_2O_3 on average) in rock-forming carbonates, apatite, and pyrochlore (Popova et al., 2017), but mostly reside in lower-temperature Ce phases (Tables 5, 13–15): monazite-(Ce), ancylite-(Ce) and REE-fluorocarbonates (synchysite-(Ce), cordylite-(Ce), and cebaite-(Ce)). Predominant La/Ce (~ 0.6–0.8) and La/Nd (~ 2–3) values in these minerals vary only slightly, which may be evidence of similar formation conditions and paragenetic relation. The almost identical shares of La, Ce and Nd cations in REE-carbonates (Fig. 11c) likewise provide evidence of general similarity in the transport mechanism and REE fractionation. The REE carrier late-magmatic fluid may have retained the PO_4/CO_3 and F/CO_3 anion ratios (Andersen et al., 2017) which led to co-precipitation of monazite and REE-carbonates. LREE might also leach from earlier REE-bearing minerals (Smith et al., 2018), but these lack signatures of intense dissolution in the Penchenga carbonatites. As shown by experiments simulating such a medium at 5–10 kb and 600–900°C, the transport and fractionation of REE may occur by complexing and hydrolysis in fluids rich in the anions of strong acids: Cl^-, F^-, and SO_4^{2-} (Hetherington et al., 2010). At 1 kb and 200–400°C, Cl^- and SO_4^{2-} behave as such ligands (Migdisov et al., 2016), while the F^- ligand in later deuteric fluids can only maintain precipitation of REE phases (Migdisov and Williams-Jones, 2014; Broom-Fendley et al., 2017). At the final stage of magmatism, the oxygen isotope systems of the associated carbonates, apatite, magnetite, and pyrochlore in the Penchenga carbonatites most likely closed within a similar range of temperatures: 480–240°C (Table 16). The composition changes of microinclusions in carbonatitic apatite record increasing contents of water in the mineralizer fluid upon its cooling from 600 to 200°C (Table 17; Fig. 15). The effect of deuteric fluids on fluorocalciopyrochlore may be responsible for its replacement by ferrocolumbite, fersmite, and Sr–Ba pyrochlore. Transition to low-temperature hydrothermal conditions could lead to the formation of thin rims and veinlets of barite and goethite in Fe sulfides, but this limited sulfate formation hardly would affect the REE transport.

The carbonatite deposit we studied is a rare case of U-, Th-, and REE-free pyrochlore and hexagonal pyrrothite magmatic mineralization. Accessory REE-carbonates and monazite formed under the effect of a late hydrothermal fluid. As we hypothesize, the fluid separated from a degassing juvenile alkali-dolomitic carbonatite melt, interacted with meteoric waters in a deep fault zone, and caused fenitization. Thus, mineral deposits of this kind should be explored and developed with regard to such signatures as tectonic setting, presence of fenite aureoles around magnesiocarbonatite bodies, as well as absence of igneous alkaline rocks. Furthermore, a special Nb–Ta concentration technology is required for efficient extraction of rare metals from U-free pyrochlore.

6. Concluding remarks and future prospects

The Neoproterozoic Penchenga linear complex in the southern Yenisei Ridge consists of several large carbonatite sheets with fenite aureoles among metamorphic rocks. The most widespread petrographic varieties are similar in mineralogy and chemistry to Mg-carbonatites that can crystallize from alkaline-dolomite melts produced by low-degree partial melting of carbonated mantle peridotite.

Rock-forming minerals in the Penchenga carbonatites make up an assemblage of ferrodolomite (predominant), calcite, phlogopite, sodic amphibole, fluorapatite, magnetite, and ilmenite, as well as magmatic sulfide and rare-metal (Nb–Ta, REE) minerals. The characteristic mineralization phases include hexagonal pyrrhotite, (U, Th, REE)-poor fluorocalciopyrochlore, monazite-(Ce) and REE(Ce)-carbonates (synchysite, cordylite, cebaite, and ancylite). Hydrothermal or supergene alteration has led to replacement of primary magmatic pyrochlore having low Ta/Nb ratios and few vacancies by Sr-Ba pyrochlore, ferrocolumbite, and fersmite. Accessory REE phases share similarity in chemistry and modes of occurrence with their late magmatic analogs from carbonatites that are carried by and precipitated from REE-bearing carbohydrothermal and deuteric fluids with δD and $\delta^{18}O$ controlled by thermal meteoric waters.

As the fluids cool down from 600 to 200°C, their H_2O content increases, which is traceable from composition changes of microinclusions in apatite from the Penchenga carbonatites. The oxygen isotope systems of the coexisting carbonates, apatite, magnetite, and pyrochlore close within a narrower temperature range of ~250 to 480°C.

Judging by their Nd and Sr isotope compositions ($\varepsilon Nd(t) \approx +6$ and $\varepsilon Sr(t) \approx -19$), the Penchenga carbonatites, as well as their Nb and REE mineralization, apparently originated from a PREMA source, while the Pb initial isotope ratios (~0.81 $^{207}Pb/^{206}Pb$; ~1.99 $^{208}Pb/^{206}Pb$) in accessory pyrrhotite indicate mixing of mantle plume (OIB) and EM 2 components, as in the case of Mesozoic-Cenozoic carbonatite-alkaline volcanoes in East Africa. On the other hand, relatively high $\delta^{18}O$ in carbonates, as well as $\delta^{34}S$ and ^{207}Pb enrichment of sulfides, suggest inputs of continental crust material to the source of metals. The sulfide phases likely originated in the lower crust at a pressure of ~8 kbar (about 30 km depth), as evidenced by coexistence of pyrrhotite with Cu-free Fe-sphalerite. These estimates are consistent with experimental data that prove the possibility for carbonatite magma to ascend with a mantle plume and to form immiscible high-pressure sulfide melts.

Yet, the results we have obtained are still insufficient for full understanding of the genesis of the Penchenga carbonatites. More insights can be gained from microtexture and trace-element data for minerals. Further study will focus on LA-ICP-MS and CL determination of trace element contents in rock-forming and accessory minerals from magnesiocarbonatite samples, with petrological implications. The analyses will be used to model the chemical evolution of Penchenga-like carbonatite systems, which will fill many knowledge gaps and provide clues to the origin of apatite, sulfide and rare-metal (Nb–Ta, REE) mineralization.

Acknowledgments

We express our sincere thanks to V.N. Markov and B.B. Sakovich for helping us in the field. We greatly appreciate the analytical work by our colleagues from the National Research Tomsk

State University (Russia) and from several institutions of the Russian Academy of Sciences: Institute of Geology and Mineralogy (Novosibirsk); Geological Institute (Moscow); Institute of Geology of Ore Deposits, Petrography, Mineralogy and Geochemistry (Moscow). The study was financially supported by the Russian Ministry of Science and Higher Education (project no. 5.8988.2017/6.7: mineralogy) and by the Russian Government (project no. 14.Y26.31.0012: geochemistry). The thoughtful and encouraging reviews by Dr. Shuan-Hong Zhang and Dr. Jindrich Kynicky are gratefully acknowledged.

References

Andersen, A.K., Clark, J.G., Larson, P.B., Donovan, J.J., 2017. REE fractionation, mineral speciation, and supergene enrichment of the Bear Lodge carbonatites, Wyoming, USA. Ore Geology Reviews 89, 780–807.

Armienti, P., Gasperini, D., 2007. Do we really need mantle components to define mantle composition? Journal of Petrology 48 (4), 693–709.

Atencio, D., Andrade, M.B., Christy, A.G., Gieré, R., Kartashov, P.M., 2010. The pyrochlore supergroup of minerals: nomenclature. The Canadian Mineralogist 48, 673–698.

Baatar, M., Ochir, G., Kynicky, J., Iizumi, S., Comin-Chiaramonti, P., 2013. Some notes on the Lugiin Gol, Mushgai Khudag and Bayan Khoshuu alkaline complexes, Southern Mongolia. International Journal of Geosciences 4, 1200–1214.

Bagdasarov, Y.A., 1979. Linear-fractured bodies of carbonatites – new subformation of ultramafic alkaline-carbonatite complexes. Doklady Akademii nauk SSSR 248 (2), 412–415.

Bagdasarov, Y.A., 2014. Some formation conditions of linear-fractured type carbonatites. Litosfera 4, 113–119.

Bataleva, Y.V., Palyanov, Y.N., Borzdov, Y.M., Sobolev, N.V., 2016a. Sulfidation of silicate mantle by reduced S-bearing metasomatic fluids and melts. Geology 44 (4), 271–274.

Bataleva, Y.V., Palyanov, Y.N., Borzdov, Y.M., Zdrokov, E.V., Sobolev, N.V., 2016b. Experimental modeling of the interaction of subducted carbonates and sulfur with mantle silicates. Doklady Earth Sciences 470 (1), 953–956.

Bell, K., Blenkinsop, J., 1989. Neodymium and strontium isotope geochemistry of carbonatites. In: Bell, K. (Ed.), Carbonatites: Genesis and Evolution. Unwin Hyman, London, pp. 278–300.

Bell, K., Simonetti, A., 2010. Source of parental melts to carbonatites–critical isotopic constraints. Mineralogy and Petrology 98, 77–89.

Bell, K., Tilton, G.R., 2001. Nd, Pb and Sr isotopic compositions of East African carbonatites: evidence for mantle mixing and plume inhomogeneity. Journal of Petrology 42 (10), 1927–1945.

Bell, K., Kjarsgaard, B.A., Simonetti, A., 1998. Carbonatites – into the twenty-first century. Journal of Petrology 39 (11/12), 1839–1845.

Bell, K., Zaitsev, A.N., Spratt, J., Fröjdö, S., Rukhlov, A.S., 2015. Elemental, lead and sulfur isotopic compositions of galena from Kola carbonatites, Russia – implications for melt and mantle evolution. Mineralogical Magazine 79 (2), 219–241.

Belyatsky, B.V., Savva, E.V., Tikhomirova, M., Grosche, G., Wall, F., 2001. Age and genesis of the Siilinjarvi Archean carbonatite complex in light of isotope data. Eleventh Annual V.M. Goldschmidt Conference. USA, Virginia, Hot Springs, Abstract 3622.

Bocharov, V.A., Frolov, S.M., 1993. Apatite-Bearing Carbonatites. KMA, Voronezh, 120 pp. (in Russian).

Bodeving, S., Williams-Jones, A.E., Swinden, S., 2017. Carbonate–silicate melt immiscibility, REE mineralising fluids, and the evolution of the Lofdal Intrusive Suite, Namibia. Lithos 268–271, 383–398.

Brod, J.A., Gaspar, J.C., de Araújo, D.P., Gibson, S.A., Thompson, R.N., Junqueira-Brod, T.C., 2001. Phlogopite and tetra-ferriphlogopite from Brazilian carbonatite complexes: petrogenetic

constraints and implications for mineral-chemistry systematics. Journal of Asian Earth Sciences 19, 265–296.

Broom‐Fendley, S., Wall, F., Spiro, B., Ullmann, C.V., 2017. Deducing the source and composition of rare earth mineralizing fluids in carbonatites: insights from isotopic (C, O, $^{87}Sr/^{86}Sr$) data from Kangankunde, Malawi. Contributions to Mineralogy and Petrology 172:96. doi: 10.1007/s00410-017-1412-7

Bühn, B., Wall, F., Le Bas, M.J., 2001. Rare-earth element systematics of carbonatitic fluorapatites, and their significance for carbonatite magma evolution. Contributions to Mineralogy and Petrology 141, 572–591.

Bulakh, A.G., Rudashevsky, N.S., Karchevsky, P.I., 1998. Native gold and silver. Sulphides and REE minerals in carbonatites from Loolekop deposit (Southern Africa). Zapiski Vsesoyuznogo Mineralogicheskogo Obshchestva 127 (3), 45–54.

Bulnaev, K.V., 2000. Heterogeneity of carbonatites of the linear type. Zapiski Vsesoyuznogo Mineralogicheskogo Obshchestva 129 (3), 1–12.

Chakhmouradian, A.R., Mitchell, R.H., 1998. Lueshite, pyrochlore and monazite-(Ce) from apatite-dolomite carbonatite, Lesnaya Varaka complex, Kola Peninsula, Russia. Mineralogical Magazine 62 (6), 769–782.

Chakhmouradian, A.R., Zaitsev, A.N., 2012. Rare earth mineralization in igneous rocks: sources and processes. Elements 8, 347–353.

Chakhmouradian, A.R., Reguir, E.P., Kressall, R.D., Crozier, J., Pisiak, L.K., Sidhu, R., Yang, P., 2015. Carbonatite-hosted niobium deposit at Aley, northern British Columbia (Canada): Mineralogy, geochemistry and petrogenesis. Ore Geology Reviews 64, 642–666.

Chakhmouradian, A.R., Reguir, E.P., Zaitsev, A.N., 2016. Calcite and dolomite in intrusive carbonatites. I. Textural variations. Mineralogy and Petrology 110, 333–360.

Chakhmouradian, A.R., Reguir, E.P., Zaitsev, A.N., Couëslan, C., Xue, C., Kynický, J., Mumin, A.H., Yang, P., 2017. Apatite in carbonatitic rocks: Compositional variation, zoning, element partitioning and petrogenetic significance. Lithos 274–275, 188–213.

Chernyshev, I.V., Chugaev, A.V., Shatagin, K.N., 2007. High Precision Pb isotope analysis by Multicollector ICP Mass Spectrometry using $^{205}Tl/^{203}Tl$ normalization: optimization and calibration of the method for the studies of Pb isotope variations. Geochemistry International 45 (11), 1065–1076.

Chernyshova, L.V. (Ed.), 1989. Typomorphism of Minerals. Nedra, Moscow, 560 pp. (in Russian).

Chiba, H., Chacko, T., Clayton, R.N., Goldsmith, J.R., 1989. Oxygen isotope fractionations involving diopside, forsterite, magnetite, and calcite: application to geothermometry. Geochimica et Cosmochimica Acta 53, 2985–2995.

Çimen, O., Kuebler, C., Monaco, B., Simonetti, S.S., Corcoran, L., Chen, W., Simonetti A., 2018. Boron, carbon, oxygen and radiogenic isotope investigation of carbonatite from the Miaoya complex, central China: Evidences for late-stage REE hydrothermal event and mantle source heterogeneity. Lithos 322, 225–237.

Conway, C.H., Taylor, H.P., 1969. $^{18}O/^{16}O$ and $^{13}C/^{12}C$ ratios of coexisting minerals in the Oka and Magnet Cove carbonatite bodies. Journal of Geology 77 (5), 618–626.

Dalsin, M.L., Groat, L.A., Creighton, S., Evans, R.J., 2015. The mineralogy and geochemistry of the Wicheeda Carbonatite Complex, British Columbia, Canada. Ore Geology Reviews 64, 523–542.

Deines, P., 1989. Stable isotope variations in carbonatites. In: Bell, K. (Ed.), Carbonatites: Genesis and Evolution. Unwin Hyman, London, pp. 301–359.

Deditius, A.P., Smith (Skomurski), F.N., Utsunomiya, S., Ewing, R.C., 2015. Role of vein-phases in nanoscale sequestration of U, Nb, Ti, and Pb during the alteration of pyrochlore. Geochimica et Cosmochimica Acta 150, 226–252.

Doroshkevich, A.G., Ripp, G., Viladkar, S., 2010. Newania carbonatites, Western India: example of mantle derived magnesium carbonatites. Mineralogy and Petrology 98, 283–295.

Doroshkevich, A.G., Ripp, G.S., Izbrodin, I.A., Savatenkov, V.M., 2012. Alkaline magmatism of the Vitim province, West Transbaikalia, Russia: Age, mineralogical, geochemical and isotope (O, C, D, Sr and Nd) data. Lithos 152, 157–172.

Eriksson, S.C., 1989. Phalaborwa: a saga of magmatism, metasomatism and miscibility. In: Bell, K. (Ed.), Carbonatites: Genesis and Evolution. Unwin Hyman, London, pp. 221–254.

Ernst, R.E., Bell, K., 2010. Large igneous provinces (LIPs) and carbonatites. Mineralogy and Petrology 98, 55–76.

Farrell, S., Bell, K., Clark, I., 2010. Sulphur isotopes in carbonatites and associated silicate rocks from the Superior Province, Canada. Mineralogy and Petrology 98, 209–226.

Feng, M., Xu, C., Kynicky, J., Zeng, L., Song, W., 2016. Rare earth element enrichment in Palaeoproterozoic Fengzhen carbonatite from the North China block. International Geology Review 58 (15), 1940–1950.

Fortier, S.M., Luttge, A., 1995. An experimental calibration of the temperature dependence of oxygen isotope fractionation between apatite and calcite at high temperatures (350–800^{o}C). Chemical Geology 125, 281–290.

Fortier, S.M., Lüttge, A., Satir, M., Metz, P., 1994. Oxygen isotope fractionation between fluorphlogopite and calcite: an experimental investigation of temperature dependence and F^{-}/OH^{-} effects. European Journal of Mineralogy 6 (1), 53–65.

Förster, H.J., 1998. The chemical composition of REE-Y-Th-U-rich accessory minerals in peraluminous granites of the Erzgebirge-Fichtelgebirge region, Germany, Part I: The monazite-(Ce)-brabantite solid solution series. American Mineralogist 83, 259–272.

Giret, A., Bonin, B., Leger, J.M., 1980. Amphibole compositional trends in oversaturated and undersaturated alkaline plutonic ring-complexes. The Canadian Mineralogist 18, 481–495.

Glevasskii, E.B., Krivdik, S.G., 1981. The Precambrian Carbonatite Complex in the Azov Area. Naukova Dumka, Kiev, 226 pp. (in Russian).

Hart, S.R., Hauri, E.H., Oschmann, L.A, Whitehead, J.A., 1992. Mantle plumes and entrainment: isotopic evidence. Science 256, 517–520.

Hetherington, C.J., Harlov, D.E., Budzyń, B., 2010. Experimental metasomatism of monazite and xenotime: mineral stability, REE mobility and fluid composition. Mineralogy and Petrology 99, 165–184.

Hogarth, D.D., 1977. Classification and nomenclature of the pyrochlore group. American Mineralogist 62, 403–410.

Hogarth, D.D., 1989. Pyrochlore, apatite and amphibole: distinctive minerals in carbonatite. In: Bell, K. (Ed.), Carbonatites: Genesis and Evolution. Unwin Hyman, London, pp. 105–148.

Hogarth, D.D., Williams, C.T., Jones, P., 2000. Primary zoning in pyrochlore group minerals from carbonatites. Mineralogical Magazine 64, 683–697.

Hou, Z.,Q., Tian, S.H., Yuan, Z.X., Xie, Y.L., Yin, S.P., Yi, L.S., Fei, H.C., Yang, Z.M., 2006. The Himalayan collision zone carbonatites in western Sichuan, SW China: petrogenesis, mantle source and tectonic implication. Earth and Planetary Science Letters 244, 234–250.

Hutchison, M.N., Scott, S.D., 1981. Sphalerite geobarometry in the Cu-Fe-Zn-S system. Economic Geology 76 (1), 143–153.

Jago, B., Gittins, J., 1993. Pyrochlore crystallization in carbonatites: the role of fluorine. South African Journal of Geology 96 (3), 149–159

Kapustin, Yu.L., 1980. Mineralogy of carbonatites. Amerind Publishing Company Pvt. Ltd., New Dehli, 259 pp.

Karchevsky, P.I., 2005. Sulfide, Strontium and Rare Earth Mineralization of Phoscorites and Carbonatites. Publishing House Kolo, St-Petersburg, 160 pp. (in Russian).

Kjarsgaard, B.A., Hamilton, D.L., 1988. Liquid immiscibility and the origin of alkali-poor carbonatites. Mineralogical Magazine 52 (1), 43–55.

Kjarsgaard, B.A., Mitchell R.H., 2008. Solubility of Ta in the system $CaCO_3$– $Ca(OH)_3$–$NaTaO_3$–$NaNbO_3$ ± F at 0.1 GPa: implications for the crystallization of pyrochlore-group minerals in carbonatites. The Canadian Mineralogist 46, 981–990.

Kjarsgaard, B.A, Hamilton, D.L, Peterson, T.D, 1995. Peralkaline nephelinite/carbonatite liquid immiscibility: comparison of phase compositions in experiments and natural lavas from Oldoinyo Lengai. In: Bell K., Keller J. (Eds), Carbonatite Volcanism. Springer, Berlin, pp. 163–190.

Kornev, T.Ya., Kachevskii, L.K., Nozhkin, A.D., Dazenko, V.M., Storozhenko, A.A., Zablozkii, K.A., Romanov, A.P., 1999. Correlation pattern of magmatic and metamorphic rock complexes in the Yenisei Range. In: Khomichov, V.L. (Ed.), Regional Correlation Patterns of Magmatic and Metamorphic Rock Complexes in the Altai-Sayan Fold Area. SRIGGMR, Novosibirsk, pp. 17–46. (in Russian)

Korobeinikov, A.N., Mitrofanov, F.P., Gehőr, S., Laajoki, K., Pavlov, V.P., Mamontov, V.P., 1998. Geology and copper sulphide mineralization of the Salmagor Ring igneous complex, Kola Peninsula, NW Russia. Journal of Petrology 39 (11/12), 2033–2041.

Kostov, I., 1968. Mineralogy. Oliver and Boyd, Edinburgh and London, 584 pp.

Kramm, U., 1993. Mantle components of carbonatites from the Kola alkaline province, Russia and Finland: A Nd-Sr study. European Journal of Mineralogy 5, 985–989.

Kramm, U., Kogarko, L.N., 1994. Nd and Sr isotope signatures of the Khibina and Lovozero agpaitic centres, Kola alkaline province, Russia. Lithos 32, 225–242.

Kuzmichev, A.B., Sklyarov, E.V., 2016. The Precambrian of Transangaria, Yenisei Ridge (Siberia): Neoproterozoic microcontinent, Grenville-age orogen, or reworked margin of the Siberian craton? Journal of Asian Earth Sciences 115 (1), 419–441.

Kynicky, J., Smith, M.P., Xu, C., 2012. Diversity of rare earth deposits: The key example of China. Elements 8, 361–367.

Lapin, A.V., Kulikova, I.M., 1989. Alteration of pyrochlore from weathered carbonatites. Zapiski Vsesoyuznogo Mineralogicheskogo Obshchestva 118 (1), 41–49.

Lapin, A.V., Ploshko, V.V., 1988. Carbonatites: types of associations and morphology and geology-tectonic conditions of formation. Izv. Akademii Nauk SSSR, Ser. Geologicheskaya, No. 1, 66–73.

Lapin, A.V., Ploshko, V.V., Malyshev, A.A., 1987. Carbonatites from the Tatarka deep fault zone, Yenisei Ridge. Geologiya Rudnykh Mestorozhdenii, No. 1, 30–45.

Lapin, A.V., Tolstov, A.V., Kulikova, I.M., 2016. Distribution of REE, Y, Sc, and Th in the unique complex rare-metal ores of the Tomtor deposit. Geochemistry International 54 (12), 1061–1078.

Leake, B.E., Woolley, A.R., Arps, C.E.S., Birch, W.D., Gilbert, M.C, Grice, J.D., Hawthorne, F.C., Kato, A., Kisch, H.J., Krivovichev, V.G., 1997. Nomenclature of amphiboles: report of the subcommittee on amphiboles of the International Mineralogical Association, Commission on new minerals and mineral names. The Canadian Mineralogist 35, 219–246.

Le Bas, M.J., Handley, C., 1979. Variation in apatite composition in ijolitic and carbonatitic igneous rocks. Nature 279, 54–56.

Le Bas, M.J., Srivastava, R.K., 1989. The mineralogy and geochemistry of the Mundwara carbonatite dykes, Sirohi District, Rajasthan, India. Neues Jahrbuch für Mineralogie Abhandlungen 160 (2), 207–227.

Lee, W-J., Wyllie, P.J., 1994. Experimental data bearing on liquid immiscibility, crystal fractionation, and the origin of calciocarbonatites and natrocarbonatites. International Geology Review 36, 797–819.

Lee, W-J., Wyllie, P.J., 1998. Petrogenesis of carbonatite magmas from mantle to crust, constrained by the system CaO-(MgO+FeO^*)-(Na_2O+K_2O)-(SiO_2+Al_2O_3+TiO_2)-CO_2. Journal of Petrology 39 (3), 495–517.

Lee, W-J., Wyllie, P.J., 2000. The system CaO-MgO-SiO_2-CO_2 at 1 GPa, metasomatic wehrlites, and primary carbonatite magmas. Contributions to Mineralogy and Petrology 138, 214–228.

Lee, M.J., Lee, J.I., Hur, S.D., Kim, Y., Moutte, J., Balaganskaya, E., 2006. Sr–Nd–Pb isotopic compositions of the Kovdor phoscorite–carbonatite complex, Kola Peninsula, NW Russia. Lithos 91, 250–261.

Levin, V. Ya., Ronenson, B.M., Samkov, V.S., Levina, I.A., Sergeev, N.S., Kiselev, A.P., 1997. Alkali-Carbonatite Complexes of the Urals. Ural Geological Committee, Ekaterinburg, 274 pp. (in Russian).

Likhanov, I.I., Nozhkin, A.D., Reverdatto, V.V., Kozlov, P.S., 2014. Grenville tectonic events and evolution of the Yenisei ridge at the western margin of the Siberian craton. Geotectonics 48 (5), 371–389.

Likhanov, I.I., Reverdatto, V.V., Kozlov, P.S., Khiller, V.V., Sukhorukov, V.P., 2015. P–T–t constraints on polymetamorphic complexes of the Yenisei Ridge, East Siberia: Implications for Neoproterozoic paleocontinental reconstructions. Journal of Asian Earth Sciences 113, 391–410.

Martin, L.H.J., Schmidt, M.W., Mattsson, H.B., Guenther, D., 2013. Element partitioning between immiscible carbonatite and silicate melts for dry and H_2O-bearing systems at 1–3 GPa. Journal of Petrology 54 (11), 2301–2338.

Mattews, A., Goldshmith, D., Clayton, R.N., 1983. Oxygen isotope fractionation between zoisite and water. Geochimica et Cosmochimica Acta 47 (3), 645–654.

Mian, I., Le Bas, M.J., 1987. The biotite-phlogopite series in fenites from the Loe Shilman carbonatite complex, NW Pakistan. Mineralogical Magazine 51 (3), 397–408.

Migdisov, A.A., Williams-Jones, A.E., 2014. Hydrothermal transport and deposition of the rare earth elements by fluorine-bearing aqueous liquids. Mineralium Deposita 49, 987–997.

Migdisov, A., Williams-Jones, A.E., Brugger, J., Caporuscio, F.A., 2016. Hydrothermal transport, deposition, and fractionation of the REE: Experimental data and thermodynamic calculations. Chemical Geology 439, 13–42.

Mitchell, R.H., Kjarsgaard, B.A., 2004. Solubility of niobium in the system $CaCO_3$–CaF_2–$NaNbO_3$ at 0.1 GPa pressure: implications for the crystallization of pyrochlore from carbonatite magma. Contributions to Mineralogy and Petrology 148, 281–287.

Mitchell, R.H., Kjarsgaard, B.A., 2011. Experimental studies of the system Na_2CO_3–$CaCO_3$–MgF_2 at 0.1GPa: implications for the differentiation and low-temperature crystallization of natrocarbonatite. Journal of Petrology 52 (7/8), 1265–1280.

Möller, P., 1989. REE (Y), Nb, and Ta enrichment in pegmatites and carbonatite-alkalic rock complexes. In: Möller et al. (Eds.), Lanthanides, Tantalum and Niobium. Springer, Berlin, pp. 38–67.

Nasraoui, M., Bilal, E., 2000. Pyrochlores from the Lueshe carbonatite complex (Democratic Republic of Congo): a geochemical record of different alteration stages. Journal of Asian Earth Sciences 18, 237–251.

Nedosekova, I.L., Vladykin, N.V., Pribavkin, S.V., Bayanova, T.B., 2009. The Il'mensky–Vishnevogorsky Miaskite–Carbonatite Complex, the Urals, Russia: Origin, Ore Resource Potential, and Sources. Geology of Ore Deposits 51 (2), 139–161.

Nedosekova, I.L., Belousova, E.A., Sharygin, V.V., Belyatsky, B.V., Bayanova, T.B., 2013. Origin and evolution of the Ilmeny-Vishnevogorsky carbonatites (Urals, Russia): insights from trace-element compositions, and Rb-Sr, Sm-Nd, U-Pb, Lu-Hf isotope data. Mineralogy and Petrology 107, 101–123.

Nedosekova, I.L., Koroteev, V.A., Bayanova, T.B., Belyatsky, B.V., 2018. Sources of ore substance of carbonatite complexes of the Ural fold belt: Rb–Sr and Sm–Nd isotope data. Doklady Earth Sciences 480 (Part 2), 773–777.

Nozhkin, A.D., Turkina, O.M., Bayanova, T.B., Berezhnaya, N.G., Larionov, A.N., Postnikov, A.A., Travin, A.V., Ernst R.E., 2008. Neoproterozoic rift and within-plate magmatism in the Yenisei Ridge: implications for the breakup of Rodinia. Russian Geology and Geophysics 49 (7), 503–519.

Osorgin, N.Yu., 1990. Chromatographic analysis of the gas phase in minerals (technique, instruments, and metrology). Preprint 11, Institut Geologii i Geofiziki SO AN SSSR, Novosibirsk, 33 pp. (in Russian).

Pokrovskii, B.G., 2000. Crustal Contamination of Mantle Magmas: Evidence from Isotope Geochemistry. Nauka, Moscow, 228 pp. (in Russian).

Pokrovskii, B.G., Andreeva, E.D., Vrublevskii, V.V., Grinev, O.M., 1998. Contamination mechanisms of alkaline-gabbro intrusions in the southern periphery of the Siberian craton: evidence from strontium and oxygen isotopic compositions. Petrologiya 6(3), 237–251.

Popova, V.I., Kozlov, P.S., Lapin, A.V., Popov, V.A., Kotllyarov, V.A., Pautov, L.A., Rassomakhin, M.A., Shilovskikh, V.V., Blinov, I.A., 2017. New data on pyrochlore from the Tatarka deposit (Yenisei Ridge, Russia). Mineralogiya 1, 23–37.

Puustinen, K., 1971. Geology the Siilinjarvi carbonatite complex, Eastern Finland. Bull. de la Commission Géologique de Finlande 249, 43 pp.

Ray, J.S., Shukla, A.D., Dewangan, L.K., 2010. Carbon and oxygen isotopic compositions of Newania Dolomite Carbonatites, Rajasthan, India: implications for source of carbonatites. Mineralogy and Petrology 98, 269–282.

Ribeiro, C.C., Brod, J.A., Junqueira-Brod, T.C., Gaspar, J.C., Petrinovic, I.A., 2005. Mineralogical and field aspects of magma fragmentation deposits in a carbonate–phosphate magma chamber: evidence from the Catalão I complex, Brazil. Journal of South American Earth Sciences 18, 355–369.

Romanova, I.V., Vernikovskaya, A.E., Vernikovsky, V.A., Matushkin, N.Yu., Larionov A.N., 2012. Neoproterozoic alkaline magmatism and associated igneous rocks in the western framing of

the Siberian craton: petrography, geochemistry, and geochronology. Russian Geology and Geophysics 53(11), 1176–1196.

Rudashevsky, N.S., Knauf, V.V., Krasnova, N.I., Rudashevsky, V.N., 1995. The first description of gold and platinum group minerals in ores and carbonatites of alkaline-ultramafic complex (Kovdor Massif, Russia). Zapiski Vsesoyuznogo Mineralogicheskogo Obshchestva 124 (5), 1–15.

Sazonov, A.M., Vrublevsky, V.V., Gertner, I.F., Fedorova, A.V., Gavrilenko, V.V., Zvyagina, E.A., Leont'ev, S.I., 2007. The Transangara alkaline pluton, Yenisei range: Rb-Sr and Sm-Nd isotope ages and sources of feldspathoid magmas in Late Precambrian. Doklady Earth Sciences 413A (3), 469–473.

Samoilov, V.S., Gormasheva, G.S., 1975. Alkali amphiboles from carbonatites and congenetic rocks. Zapiski Vsesoyuznogo Mineralogicheskogo Obshchestva 104 (2), 145–159.

Samoilov, V.S., 1984. Geochemistry of Carbonatites. Nauka, Moscow, 191 pp. (in Russian).

Seifert, W., Kämpf, H., Wasternack, J., 2000. Compositional variation in apatite, phlogopite and other accessory minerals of the ultramafic Delitzsch complex, Germany: implication for cooling history of carbonatites. Lithos 53, 81–100.

Smith, M.P., Henderson, P., Campbell, L.S., 2000. Fractionation of the REE during hydrothermal processes: constraints from the Bayan Obo Fe-REE-Nb deposit, Inner Mongolia, China. Geochimica et Cosmochimica Acta 64 (18), 3141–3160.

Smith, M., Kynicky, J., Xu, C., Song, W., Spratt, J., Jeffries, T., Brtnicky, M., Kopriva, A., Cangelosi, D., 2018. The origin of secondary heavy rare earth element enrichment in carbonatites: Constraints from the evolution of the Huanglongpu district, China. Lithos 308–309, 65–82.

Sobachenko, V.N., Plyusnin, G.S., Sandimirova, G.P., Pakhol'chenko, Yu.A., 1986. Rb-Sr age of circumfracture alkaline metasomatites and granites of the Tatarka-Penchenga zone, Yenisei Range. Doklady Akademii Nauk SSSR 287(5), 1220–1224.

Song, W., Xu, C., Veksler, I.V., Kynicky J., 2016. Experimental study of REE, Ba, Sr, Mo and W partitioning between carbonatitic melt and aqueous fluid with implications for rare metal mineralization. Contributions to Mineralogy and Petrology 171:1.

Song, W., Xu, C., Chakhmouradian, A.R., Kynicky, J., Huang, K., Zhang, Z., 2017. Carbonatites of Tarim (NWChina): First evidence of crustal contribution in carbonatites from a large igneous province. Lithos 282–283, 1–9.

Stacey, J.C., Kramers, J.D., 1975. Approximation of terrestrial lead isotope evolution by a two-stage model. Earth and Planetary Science Letters 26, 207–221.

Stracke, A., Hofmann, A.W., Hart, S.R., 2005. FOZO, HIMU, and the rest of the mantle zoo. Geochemistry, Geophysics, Geosystems 6 (5), Q05007.

Taylor, H.P., Frechen, J., Degens, E.T., 1967. Oxygen and carbon isotope studies of carbonatites from the Laacher See district, West Germany and Alnö district, Sweden. Geochimica et Cosmochimica Acta 31 (3), 407–430.

Tichomirowa, M., Grosche, G., Götze, J., Belyatsky, B.V., Savva, E.V., Keller, J., Todt, W., 2006. The mineral isotope composition of two Precambrian carbonatite complexes from the Kola alkaline province – alteration versus primary magmatic signatures. Lithos 91, 229–249.

Tilton, G.R., Bryce, J.G., Mateen, A., 1998. Pb-Sr-Nd isotope data from 30 and 300 Ma collision zone carbonatites in Northwest Pakistan. Journal of Petrology 39 (11/12), 1865–1874.

Ting, W., Rankin, A.H., Woolley, A.R., 1994. Petrogenetic significance of solid carbonate inclusions in apatite of the Sukulu carbonatite, Uganda. Lithos 31, 177–187.

Tremblay, J., Bédard, L. P., Matton, G., 2017. Columbitization of fluorocalciopyrochlore by hydrothermalism at the Saint-Honoré alkaline complex, Québec (Canada): New insights on halite in carbonatites. Ore Geology Reviews 91, 695–707.

Trofanenko, J., Williams-Jones, A.E., Simandl, G.J., Migdisov, A.A., 2016. The nature and origin of the REE mineralization in the Wicheeda carbonatite, British Columbia, Canada. Economic Geology 111, 199–223.

Veksler, I.V., Petibon, C., Jenner, G.A., Dorfman, A.M., Dingwell, D.B., 1998a. Trace element partitioning in immiscible silicate-carbonate liquid systems: an initial experimental study using a centrifuge autoclave. Journal of Petrology 39 (11–12), 2095–2104.

Veksler, I.V., Nielsen, T.F.D., Sokolov, S.V., 1998b. Mineralogy of crystallised melt inclusions from Gardiner and Kovdor ultramafic alkaline complexes: implications for carbonatite genesis. Journal of Petrology 39 (11–12), 2015–2031.

Vernikovsky, V.A., Vernikovskaya, A.E., 2006. Tectonics and evolution of granitoid magmatism of the Yenisei Ridge. Russian Geology and Geophysics 47 (1), 35–52.

Vernikovsky, V.A., Vernikovskaya, A.E., Kotov, A.B., Salnikova, E.B., Kovach, V.P., 2003. Neoproterozoic accretionary and collisional events on the western margin of Siberian craton: new geological and geochronological evidence from the Yenisei Range. Tectonophysics 375, 147–168.

Vernikovsky, V.A., Vernikovskaya, A.E., Sal'nikova, E.B., Berezhnaya, N.G., Larionov, A.N., Kotov, A.B., Kovach, V.P., Vernikovskaya, I.V., Matushkin, N.Yu., Yasenev, A.M., 2008. Late Riphean alkaline magmatism in the western margin of the Siberian craton: a result of continental rifting or accretionary events? Doklady Earth Sciences 419 (2), 226–230.

Vernikovsky, V.A., Kazansky, A.Yu., Matushkin, N.Yu., Metelkin, D.V., Sovetov, J.K., 2009. The geodynamic evolution of the folded framing and the western margin of the Siberian craton in the Neoproterozoic: geological, structural, sedimentological, geochronological, and paleomagnetic data. Russian Geology and Geophysics 50 (4), 380–393.

Viladkar, S.G., 1998. Carbonatite occurrences in Rajasthan, India. Petrologiya 6 (3), 295–306.

Viladkar, S.G., Wimmenauer, W., 1986. Mineralogy and geochemistry of the Newania carbonatite-fenite complex, Rajasthan, India. Neues Jahrbuch für Mineralogie – Abhandlungen 156 (1), 1–21.

Vrublevskii, V.V., 2015. Sources and geodynamic setting of petrogenesis of the Middle Cambrian Upper Petropavlovka alkaline basic pluton (Kuznetsk Alatau, Siberia). Russian Geology and Geophysics 56 (3), 379–401.

Vrublevskii, V.V., Babanskii, A.D., Troneva, N.V., Elisafenko, V.N., 1989. Mineral-forming conditions in carbonatites of the Kuznetsk Alatau. Izv. Akademii Nauk SSSR, Ser. Geologicheskaya, No. 12, 65–81.

Vrublevskii, V.V., Pokrovskii, B.G., Zhuravlev, D.Z., Anoshin, G.N., 2003. Composition and age of the Penchenga linear carbonatite complex, Yenisei Range. Petrology 11 (2), 130–146.

Vrublevskii, V.V., Reverdatto, V.V., Izokh, A.E., Gertner, I.F., Yudin, D.S., Tishin, P.A., 2011. Neoproterozoic carbonatite magmatism of the Yenisei Ridge, Central Siberia: $^{40}Ar/^{39}Ar$ geochronology of the Penchenga rock complex. Doklady Earth Sciences 437 (2), 443–448.

Vrublevskii, V.V., Krupchatnikov, V.I., Izokh, A.E., Gertner, I.F., 2012. The alkaline and carbonatitic rocks of Gorny Altai (Edel'veis complex) as indicators of Early Paleozoic plume magmatism in the Central Asian Fold Belt. Russian Geology and Geophysics 53, 721–735.

Vrublevskii, V.V., Krupchatnikov, V.I., Gertner, I.F., 2017. The role of the mantle in Early Paleozoic oceanic-island volcanism: evidence from OIB geochemistry in the SE Altai Mountains. Geosfernye Issledovaniya, No. 1, 28–38.

Vrublevskii, V.V., Morova, A.A., Bukharova, O.V., Konovalenko, S.I., 2018a. Mineralogy and geochemistry of Triassic carbonatites in the Matcha alkaline intrusive complex (Turkestan-Alai Ridge, Kyrgyz Southern Tien Shan), SW Central Asian orogenic belt. Journal of Asian Earth Sciences 153, 252–281.

Vrublevskii, V.V., Gertner, I.F., Chugaev, A.V., 2018b. Parental sources of high–alumina alkaline melts: Nd, Sr, Pb, and O isotopic evidence from the Devonian Kiya–Shaltyr gabbro–urtite intrusion, South Siberia. Doklady Earth Sciences 479, part 2, 518–523.

Vrublevskii, V.V., Nikiforov, A.V., Sugorakova, A.M., Kozulina, T.V., 2019a. Mantle-crustal origin of Early Paleozoic alkaline intrusions from Central Sangilen, SE Tuva: Nd, Sr, Pb, C, O isotope data. Russian Geology and Geophysics 60, 635–650.

Vrublevskii, V.V., Gertner, I.F., Ernst, R.E., Izokh, A.E., Vishnevskii, A.V., 2019b. The Overmaraat-Gol alkaline pluton in Northern Mongolia: U–Pb age and preliminary implications for magma sources and tectonic setting. Minerals 9(3), 170.

Wall, F., Zaitsev, A.N. (Eds.), 2004. Phoscorites and Carbonatites from Mantle to Mine: the Key Example of the Kola Alkaline Province. The Mineralogical Society of Great Britain and Ireland. The Mineralogical Society, Ser. 10, 516 pp.

Wall, F., Williams, C.T., Woolley, A.R., 1996. Pyrochlore from weathered carbonatite at Lueshe, Zaire. Mineralogical Magazine 60, 731–750.

Wallace, M.E., Green, D.H., 1988. An experimental determination of primary carbonatite magma composition. Nature 335, 343–346.

Wang, L., Xu, C., Zhao, Z., Song, W., Kynicky, J., 2015. Petrological and geochemical characteristics of Zhaibei granites in Nanling region, Southeast China: implications for REE mineralization. Ore Geology Reviews 64, 569–582.

Williams-Jones, A.E., Migdisov, A.A., Samson, I.M., 2012. Hydrothermal mobilisation of the rare earth elements – a tale of "Ceria" and "Yttria". Elements 8, 355–360.

Williams, C.T., 1996. The occurrence of niobian zirconolite, pyrochlore and baddeleyite in the Kovdor carbonatite complex, Kola Peninsula, Russia. Mineralogical Magazine 60, 639–646.

Wyllie, P.J., Lee, W-J., 1998. Model system controls on conditions for formation of magnesiocarbonatite and calciocarbonatite magmas from the mantle. Journal of Petrology 39 (11/12), 1885–1893.

Woolley, A.R., Kempe, D.R.C., 1989. Carbonatites: Nomenclature, average chemical compositions, and element distribution. In: Bell, K. (Ed.), Carbonatites: Genesis and Evolution. Unwin Hyman, London, pp. 1–14.

Woolley, A.R., Kjarsgaard, B.A., 2008a. Carbonatite occurrences of the world: map and database. Geological Survey of Canada Open File 5796, 28 p.

Woolley, A.R., Kjarsgaard, B.A., 2008b. Paragenetic types of carbonatite as indicated by the diversity and relative abundances of associated silicate rocks: evidence from a global database. The Canadian Mineralogist 46(4), 741–752.

Wu, F.Y., Mitchell, R.H., Li, Q.L., Zhang, C., Yang, Y.H., 2017. Emplacement age and isotopic composition of the Prairie Lake carbonatite complex, northwestern Ontario, Canada. Geological Magazine 154 (2), 217–236.

Xu, C., Campbell, I.H., Kynicky, J., Allen, C.M., Chen, Y., Huang, Z., Qi, L., 2008. Comparison of the Daluxiang and Maoniuping carbonatitic REE deposits with Bayan Obo REE deposit, China. Lithos 106, 12–24.

Xu, C., Kynicky, J., Chakhmouradian, A.R., Campbell, I.H., Allen, C.M., 2010. Trace-element modeling of the magmatic evolution of rare-earth-rich carbonatite from the Miaoya deposit, Central China. Lithos 118, 145–155.

Xu, C., Chakhmouradian, A.R., Taylor, R.N., Kynicky, J., Li, W., Song, W., Fletcher, I.R., 2014. Origin of carbonatites in the South Qinling orogen: Implications for crustal recycling and timing of collision between the South and North China Blocks. Geochimica et Cosmochimica Acta 143, 189–206.

Xu, C., Chakhmouradian, A.R., Kynicky, J., Li, Y., Song, W., Chen, W., 2019. A Paleoproterozoic mantle source modified by subducted sediments under the North China craton. Geochimica et Cosmochimica Acta 245, 222–239.

Xue, S., Ling, M.X., Liu, Y.L., Sun, W., 2018. Recycling of subducted carbonates: Formation of the Taohuala Mountain carbonatite, North China Craton. Chemical Geology 478, 89–101.

Yaroshevskii, A.A., Bagdasarov, Yu.A., 2008. Geochemical diversity of minerals of the pyrochlore group. Geochemistry International 46 (12), 1245–1266.

Zabrodin, V.Yu., Malyshev, A.A., 1975. A new complex of alkaline-mafic rocks and carbonatites in the Yenisei Range. Doklady Akademii Nauk SSSR 223 (5), 1223–1226.

Zaitsev, A.N., Sinai, M.Yu., Chakhmouradian, A.R., Lepekhina, E.N., 1998a. Pyrrhotite-pyrite assemblages in carbonatite rocks from the Khibiny alkaline massif. Russian Mineralogical Society (Zapiski RMO) 127(4), 110–119.

Zaitsev, A.N., Wall, F., Le Bas, M.J., 1998b. REE-Sr-Ba minerals from the Khibiny carbonatites, Kola Peninsula, Russia: their mineralogy, paragenesis and evolution. Mineralogical Magazine 62 (2), 225–250.

Zaitsev, A.N., Williams, Ch.T., Wall, F., Zolotarev, A.A., 2011. Chemistry evolution of pyrochlore group minerals in phoscorites and carbonatites of the Khibiny alkaline massif. Russian Mineralogical Society (Zapiski RMO) 140(3), 40–55.

Zartman, R.E., Doe, B.R., 1981. Plumbotectonics – the model. Tectonophysics 75, 135–162.

Zhu, X.K., O'Nions, R.K., 1999. Monazite chemical composition: some implications for monazite geochronology. Contributions to Mineralogy and Petrology 137, 351–363.

Zindler, A., Hart, S.R., 1986. Chemical geodynamics. Annual Review of Earth and Planetary Sciences 14, 493–571.

Zozulya, D.R., Bayanova, T.B., Serov, P.N., 2007. Age and isotopic geochemical characteristics of Archean carbonatites and alkaline rocks of the Baltic shield. Doklady Earth Sciences 415A (6), 874–879.

Zurevinski, S.E., Mitchell, R.H., 2004. Extreme compositional variation of pyrochlore-group minerals at the Oka carbonatite complex, Quebec: evidence of magma mixing? The Canadian Mineralogist 42, 1159–1168.

Figure captions

Fig. 1. Geological map of the Penchenga fenite-carbonatite complex (see Inset for location). a: Tectonic sketch of the Yenisei Ridge, after (Vernikovsky et al., 2003). Regional fault zones: *1*

– Ishimba, *2* – Tatarka, *3* – Yenisei, *4* – Nizhneangarsk, *5* – Isakovka, *6* – Angara-Bakhta. Proterozoic metasedimentary and volcanic-sedimentary deposits from terrane are shown as well: *EAT* = East Angara, *CAT* = Central Angara, *IT* = Isakovka, *PT* = Predivinsk and Archean-Paleoproterozoic granulites, amphibolites and gneisses from the Angara-Kan terrane (*AKT*). b: Location and structure of the Penchenga fenite-carbonatite complex, after Lapin et al. (1987) and Vrublevskii et al. (2011).

Fig. 2. Structure varieties of the Penchenga carbonatites. a: homogeneous massive structure formed by euhedral grains of carbonate, phlogopite, amphibole and apatite; b: trachytic structure formed by linearly oriented amphibole prismatic crystals; c: pegmatitic structure formed by cataclastic coarse grains of ferrodolomite; d–f: banded distribution of melanocratic minerals; g: massive structure of glimmerite-like rock; h: impregnation of sulfides and rare small grains of light brown pyrochlore in the apatite-phlogopite-carbonate matrix. All photographs taken with the camera Sony α 77.

Fig. 3. Petrography of the Penchenga fenite-carbonatite complex. a: glimmerite-like rock composed of euhedral phlogopite (Phl), sodic amphibole (Amp) and apatite (Ap), in plane-polarized light (PPL); b: intergranular distribution of amphibole prismatic crystals in predominantly carbonate (Cb) aggregate with phlogopite for fenites (PPL); c–d: banded distribution of amphibole prismatic crystals along ferrodolomite (Dol), apatite and magnetite (Mgt) grain boundaries in carbonatites (cross-polarized light, CPL); e–f: mosaic ferrodolomite crystal aggregate containing euhedral sodic amphibole, phlogopite and apatite in carbonatites (CPL); g–h: pyrrhotite (Po) aggregate in carbonatites. Plain light digital scanned images.

Fig. 4. Chemistry of micas (apfu) from the Penchenga complex in terms of Al, Fe(t) and Mg (a) (Brod et al., 2001), and Si vs. Al (b) (Seifert et al., 2000). Fe(t) is total iron calculated as Fe^{2+}. Carbonatites (1); lenses (“glimmerites”) along contacts of carbonatite bodies (2); fenites (3). Compositions of micas in mantle ferrodolomite carbonatites from the Newania (*N* area)

linear complex of India (Viladkar and Wimmenauer, 1986; Doroshkevich et al., 2010) are shown for reference.

Fig. 5. Chemistry of amphiboles in the Penchenga carbonatites and fenites. Carbonatites (1); schlieren ("glimmerites") in contacts of carbonatite bodies (2); fenites (3). a: Classification diagram, after (Leake et al., 1997); b: Classification diagram, after (Giret et al., 1980). Abbreviations refer to mineral names: Arf=arfvedsonite, Rct=richterite, Wnc=winchite, Rbk=riebeckite; c: Ratio of Ca, Fe(t) and Mg cations. Solid line contours prevalent amphiboles in carbonatites, after (Le Bas and Srivastava, 1989). Dashed line contours amphiboles in the Newania fenite-carbonatite linear complex of India (Viladkar and Wimmenauer, 1986; Doroshkevich et al., 2010). d: inverse correlation between Mg and Fe(t) cations in associated rock-forming amphiboles and micas.

Fig. 6. BSE (backscattered electron) image of accessory ore mineralization areas in the Penchenga carbonatites. a–b: subhedral pyrochlore (Pcl) with inclusions of apatite (Ap) and amphibole (Amp) accompanied by phlogopite (Phl), ferrodolomite (Dol), pyrrhotite (Po) and monazite (Mnz); c: ilmenite in magnetite as long exsolution lamellae; d: magnetite (Mag) grains with oriented inclusions of apatite, amphibole and anhedral ilmenite (Ilm); e–f: corrosion relationship of ilmenite, magnetite, apatite and amphibole; g–n: relationship of pyrrhotite and others sulfides (Py=pyrite, Ccp=chalcopyrite, Sp=sphalerite, Gn=galena) associated with ferrodolomite. Ank=ankerite, Cal= calcite, Gth=goethite, and Brt=barite. o–q: morphological features of REE-carbonates: (o) ancylite (Anc) microingrowths in calcite; (p–q) acicular and anhedral crystalline aggregates of synchysite (Syn) in calcite and strontianite (Str).

Fig. 7. Crystal morphology of pyrochlore in the Penchenga carbonatites. a–c: octahedral crystals with reduced hexahedral and rhombododecahedral faces, photographs of weathered rocks; d–e: sculpture of faces with stepped surfaces in crystal intergrowths (d) and plain surface in a penetration twin (e); single crystals from weathered rocks (photographs in insets) are

shown as well; f–g: euhedral and subhedral pyrochlore grains accompanied by amphibole, phlogopite; apatite and carbonate (PPL); h–i: skeleton-like pyrochlore crystals in carbonate rocky matrix (image h, CPL and image i, PPL).

Fig. 8. Chemistry of pyrochlore in the Penchenga complex (apfu). Pyrochlore I from trachytic carbonatites (1); pyrochlore II from pegmatitic carbonatites (2); pyrochlore III and supergene Sr-Ba pyrochlore from carbonatites (3). a: diagram Nb–(Ti+Zr)–Ta, after (Hogarth, 1977; Atencio et al., 2010); b: diagram Ca–*VA*–Na, after (Nasraoui and Bilal, 2000; Deditius et al., 2015). Dashed lines show the primary trend of magmatic (M) pyrochlore and increase in the amount of vacancies (*VA*, see Table 7) during transitional (hydrothermal, H) and secondary (supergene, W) alteration of pyrochlore. Ta- and Ti-poor pyrochlore compositions in carbonatites from Newania (N, India) and Lueshe (L, Africa) complexes (Viladkar, 1998; Nasraoui and Bilal, 2000) are shown for reference.

Fig. 9. XRD spectra of pyrochlore (*a*) and pyrrhotite (*b*) from the Penchenga carbonatites. See text for explanation.

Fig. 10. Fe vs. S for pyrrhotite in carbonatites. Ideal monoclinic and hexagonal pyrrhotites are plotted for reference. Pyrrhotite composition in carbonatite rocks from the alkaline plutons of Khibiny, Kovdor, Phalaborwa (Rudashevsky et al., 1995; Bulakh et al., 1998; Zaitsev et al., 1998a) are shown for reference. See text for explanation.

Fig. 11. Chemistry of monazite and REE-carbonates in the Penchenga complex. a: contents of major oxides in minerals; b: ternary diagram showing relative La_2O_3, Ce_2O_3, and Nd_2O_3 (wt. %) contents in monazite. Monazite compositions in carbonatites of other localities worldwide are plotted for reference: Siberian craton (Tomtor rare-metal deposit), China craton with Qinling and Mianning-Dechang orogenic belts (Bayan Obo, Dashigou, Yuantao, Miaoya, Daluxiang and Maoniuping), Brasília mobile belt (Catalao) and Canadian Cordillera (Wicheeda) (Zhu and O'Nions, 1999; Smith et al., 2000; Ribeiro et al., 2005; Xu et al., 2008, 2010; Dalsin et al., 2015; Lapin et al., 2016; Smith et al., 2018). Monazite compositions in

granite complexes from China and Germany (Förster, 1998; Zhu and O'Nions, 1999; Wang et al., 2015) are shown for comparison; c: ternary diagram with major REE cation vertices showing REE-carbonate compositions. Gray field marks the predominant trend of HREE-depleted fluorocarbonates from the Bear Lodge hypabyssal carbonatite-alkaline complex, Wyoming, USA (Andersen et al., 2017).

Fig. 12. The Nd–Sr–Pb isotope composition of minerals, alkaline rocks and carbonatites from the Yenisei Ridge and some other localities in Eurasia. a: $\varepsilon_{Nd}(t)$ vs. $\varepsilon_{Sr}(t)$ plot for the Penchenga magnesiocarbonatites. Gray field shows predominant compositions of nearly synchronous alkaline intrusions on the Yenisei Ridge (Sazonov et al., 2007; Romanova et al., 2012). Rock compositions of linear carbonatite-alkaline complexes of different ages in cratons (Siilinjarvi, Baltic Shield (Belyatsky et al., 2001; Zozulya et al., 2007)) and orogens (Ilmen–Vishnevogorsk and Central alkaline belt intrusions, the Urals (Nedosekova et al., 2013)); Loe Shilman and Sillai Patti complexes, Northern Pakistan (Tilton et al., 1998), are shown for comparison. b–d: Pb-Pb diagrams for sulfides, K-feldspar and rocks. Black asterisks mark pyrrhotite from the Penchenga carbonatite; *KA&GA* stands for pyrrhotite and pyrite, feldspar and whole rock data of the Kuznetsk Alatau and Russian Altai alkaline intrusions (Vrublevskii et al., 2017, 2018b); K = galena from carbonatites of the Kovdor, Sallanlatvi, Seblyavr, and Vuoriyarvi plutons in the Kola alkaline province (Bell et al., 2015). The mantle components of PREMA (Prevalent Mantle), FOZO (Focus Zone), HIMU (High-μ), DMM (Depleted MORB Mantle), EM1 (Enriched Mantle 1) and EM2 (Enriched Mantle) reservoirs, elements of plumbotectonics and lead isotope evolution in mantle and crust are according to (Stacey and Kramers, 1975; Zartman and Doe, 1981; Zindler and Hart, 1986; Hart et al., 1992; Stracke et al., 2005; Armienti and Gasperini, 2007). Abbreviations in panel (b) stand for UC = upper crust, Oro = Orogenic, M = Mantle. *EACL* = East African Carbonatite Line, after Bell and Tilton (2001).

Fig. 13. $\delta^{13}C_{PDB}$ vs. $\delta^{18}O_{SMOW}$ (a), and $\delta^{34}S_{CDT}$ (b) plots for rock-forming carbonates and sulfides in carbonatites. The compositions of primary carbonatites are after Taylor et al. (1967) and Conway and Taylor (1969). Gray squares mark predominant ferrodolomite compositions of the Penchenga complex (Lapin et al., 1987; Vrublevskii et al., 2003); N = dolomite from the Newania carbonatites, India (Viladkar, 1998; Ray et al., 2010); S = the Siilinjarvi carbonatites, Finland (Tichomirowa et al., 2006); SQ = carbonatite dikes from the Qinling orogenic belt, China (Xu et al., 2014); W = Wicheeda dolomite carbonatites, Canada (Trofanenko et al., 2016). Sulfur isotope composition is shown for sulfides in carbonatite complexes of the North America (Superior, Quebec, Magnet Cove), Eurasia (KP=Kola province, MKP=Maimecha-Kotui province, Urals, East Sayan, Yenisei Ridge (Penchenga) and SDP=Sette-Daban province) and South Africa (Palaborwa), after (Deines, 1989; Vrublevskii et al., 2003; Farrell et al., 2010; Bell et al., 2015).

Fig. 14. Penchenga magnesiocarbonatites in ternary classification diagram (a) and on isobaric liquidus surface in the model system (SiO_2 + Al_2O_3) – (CaO + Na_2O + K_2O) – (MgO + FeOt) – CO_2 (Wyllie and Lee, 1998) (b). I-III are compositions of calciocarbonatites (I), magnesiocarbonatites (II) and ferrocarbonatites (III), after Woolley and Kempe (1989). Solid line in panel *b* separates the fields of carbonate and silicate liquidus surfaces; liquid at the invariant point *Q* coexists with dolomite (Mg-calcite) and major lherzolite mineral phases at a pressure of 2.8 GPa and a temperature of 1230°C. The gray area shows the compositions of experimental carbonatite melts in equilibrium with mantle phlogopite- and amphibole-bearing lherzolites (e.g., Wallace and Green, 1988; Wyllie and Lee, 1998 and references therein).

Fig. 15. Evolution of fluid chemistry at the origin of magmatic magnesiocarbonatite: evidence from micro-inclusions in rock-forming apatite. See Table 19 and text for explanation.

Fig. 16. Mineral paragenesis in the Penchenga carbonatites.

Fig. 17. Chondrite-normalized REE patterns (a) and primitive mantle-normalized (Sun and McDonough, 1989) multi-element diagrams (b) of the Penchenga carbonatites and some other worldwide dolomite carbonatite complexes. Trace-element patterns of pegmatitic, banded trachytoid, and trachytoid varieties of the Penchenga rocks. Average dolomite carbonatite compositions in Newania and Aley complexes from India and Canada (Viladkar, 1998; Chakhmouradian et al., 2015), and world average dolomite carbonatite (Woolley and Kempe, 1989) are shown for comparison. c: (La+Ce+Pr)/REE – La/Dy_{cn} diagram (after Smith et al., 2018 and references therein). REE-ratios for Penchenga rocks, Huanglongpu REE mineralized carbonatites (Qinling Mountains, China), Bachu (Tarim basin, NW China), Bear Lodge (Wyoming province, North America), and other typical carbonatites worldwide, compared.

Tables

Table 1 Representative major-element compositions of rock-forming Ca–Mg–Fe carbonates and strontianite, Penchenga complex.

Note. [a] is 1.63 wt. % Na_2O. [b] is 1.45 wt. % BaO. [c] is 0.31 wt. % Na_2O. [d] is 2.04 wt. % BaO. (–) is below detection limit. Av=average composition; numerals in braces show number of analyses.

Table 2 Representative major-element compositions of mica, Penchenga carbonatites.

Note. 1–7 = carbonatites; 8–10 = glimmerite shlieren at contacts of carbonatite bodies. Mg# = Mg/(Mg +ΣFe). Atoms per formula units (apfu) are based on 12 oxygens. (–) is below detection limit.

Table 3 Representative major-element compositions of mica and amphibole, Penchenga fenites.

Note. *Amp* = amphibole; *Mica* = dark mica. Mg# = Mg/(Mg +ΣFe). Atoms per formula units (apfu) of amphiboles are based on 23 oxygens. (–) is below detection limit.

Table 4 Representative major-element compositions of amphibole, Penchenga carbonatites.

Note. 1–8 = carbonatites; 9-11 = glimmerite shlieren at contacts of carbonatite bodies. Atoms per formula units (apfu) are based on 23 oxygens. Mg# = Mg/(Mg +ΣFe). (–) is below detection limit.

Table 5 Representative major-element compositions of apatite and monazite-(Ce), Penchenga carbonatites.

Note. [a] is 0.10 wt. % FeO(t). [b] is 0.14 wt. % FeO(t). [c] is 0.41 wt. % FeO(t); 0.97 wt. % Ln_2O_3 (Lapin et al., 1987). [d] is 0.64 wt. % FeO(t). (–) is below detection limit. Atoms per formula units (apfu) are calculated according to the number of cations (8 for apatite and 2 for monazite).

Table 6 Representative major-element compositions of magnetite and related ilmenite, Penchenga carbonatites, sample 50/290.

Note. *Ilm* = ilmenite; *Mag* = magnetite. (–) is below detection limit.

Table 7 Representative major-element compositions of pyrochlore group minerals, Penchenga carbonatites.

Note. 1–5 = pyrochlore I from trachytic carbonatites; 6–8 = pyrochlore II from pegmatitic carbonatites; 9–12 = Sr-Ba pyrochlore III; 13, 14 = supergene Sr-Ba and Sr pyrochlore from weathered carbonatites. [a] is 2.93 wt. % UO_2, 0.04 apfu; [b] is 1.00 wt. % Ce_2O_3, 0.02 apfu. (–) is below detection limit. Atoms per formula units (apfu) are based on $A_{2-m}B_2X_{6-w}Y_{1-n}{\cdot}pH_2O$, where m=0–1.7, w=0–0.7, n=0–1, p=0–2 (Hogarth, 1977; Atencio et al., 2010). VA is number of vacancies at the A-site.

Table 8 XRD data for pyrochlore and pyrrhotite, Penchenga carbonatites.

Table 9 Representative major-elements of ferrocolumbite and fersmite, Penchenga carbonatites.

Note. 1-5 = ferrocolumbite from pegmatitic carbonatites (1, 2; sample 72/182), (3, after Lapin et al., 1987) and from weathered carbonatites (4, 5). 6 = fersmite, 1.74 wt. % Ce_2O_3, 0.03 apfu. (–) is below detection limit. Atoms per formula unit (apfu) are based on 6 oxygens.

Table 10 Representative major-element compositions of sulfides, Penchenga carbonatites.

Note. 1-3 = pyrrhotite; 4-6 = pyrite; 7-9 = chalcopyrite; 10 = galena; 11-13 = sphalerite. (–) is below detection limit. Numerals in braces show number of analyses.

Table 11 Representative major-element compositions of Ag-bearing sulfides and tellurides, Penchenga carbonatites.

Note. 1 = argentite; 2-3 = argentopentlandite; 4 = hessite. (–) is below detection limit. Numerals in braces are number of analyses.

Table 12 Chemical composition of synchysite-(Ce) and ancylite-(Ce) in carbonatites.

Note. Atoms per formula units (apfu) are calculated by the number of cations. (–) is below detection limit. Numerals in braces show number of analyses. Ideal formula for synchysite: $Ca(Ce, La)(CO_3)_2F$. Ideal formula for ancylite: $Sr(Ce, La)(CO_3)_2(OH)\times H_2O$. Synchysite and ancylite from the Khibiny and Wicheeda carbonatites, after Zaitsev et al. (1998a) and Dalsin et al. (2015) respectively.

Table 13 Chemical composition of cordylite-(Ce) and cebaite-(Ce) in carbonatites.

Note. 1-3, 5, 7 = cordylite; 4, 6, 8 = cebaite. [a] is 0.25 wt. % FeO(t); [b] is 0.48 wt. % FeO(t). Atoms per formula units (apfu) are calculated according to the number of cationic positions (4 for cordylite and 5 for cebaite). (–) is below detection limit. Numerals in braces are number of analyses. Ideal formulae are $(Na, Ca)Ba(Ce, La)_2(CO_3)_4F$ for cordylite-(Ce) and $Ba_3Ce_2(CO_3)_5F_2$ for cebaite-(Ce). Cordylite and cebaite from Khibiny and Wicheeda carbonatites, after Zaitsev et al. (1998a) and Dalsin et al. (2015) respectively.

Table 14 Sr–Nd isotopic composition of the Penchenga carbonatites.

Note. Primary (T=725 Ma) isotope ratios, ε_{Nd} and ε_{Sr}, after (Vrublevskii et al., 2003, 2011).

Table 15 Pb isotopic composition of pyrrhotite, Penchenga carbonatites.

Note. U/Pb = 0.28, Th/Pb = 0.045. *m*=measured Pb isotopic ratios, *in*=initial (725 Ma) Pb isotopic ratios.

Table 16 Isotopic composition of O, C and H (in permil, ‰) and equilibrium temperatures for the minerals of Penchenga carbonatites.

Note. Data after Vrublevskii et al., 2003. Isotopic temperatures were calculated from the relationship: $1000 \ln\alpha$ (calcite-magnetite) $= 5.91 \times 10^6/T^2$ (Chiba et al., 1989); $1000 \ln\alpha$ (calcite-apatite) $= 1.6 \times 10^6/T^2$ (Fortier and Luttge, 1995); $1000 \ln\alpha$ (calcite-phlogopite) $= 1.84 \times 10^6/T^2$ (Fortier et al., 1994); $1000 \ln\alpha$ (calcite-pyrochlore) $= 5.61 \times 10^6/T^2$ (Mattews et al., 1983).

Table 17 Fluid phase composition (mg/kg) from micro-inclusions in apatite, Penchenga carbonatites.

Table 18 Average major- and trace-element concentrations, Penchenga carbonatite varieties.

Note. Data after Vrublevskii et al., 2003. Numerals in braces show number of analyses.

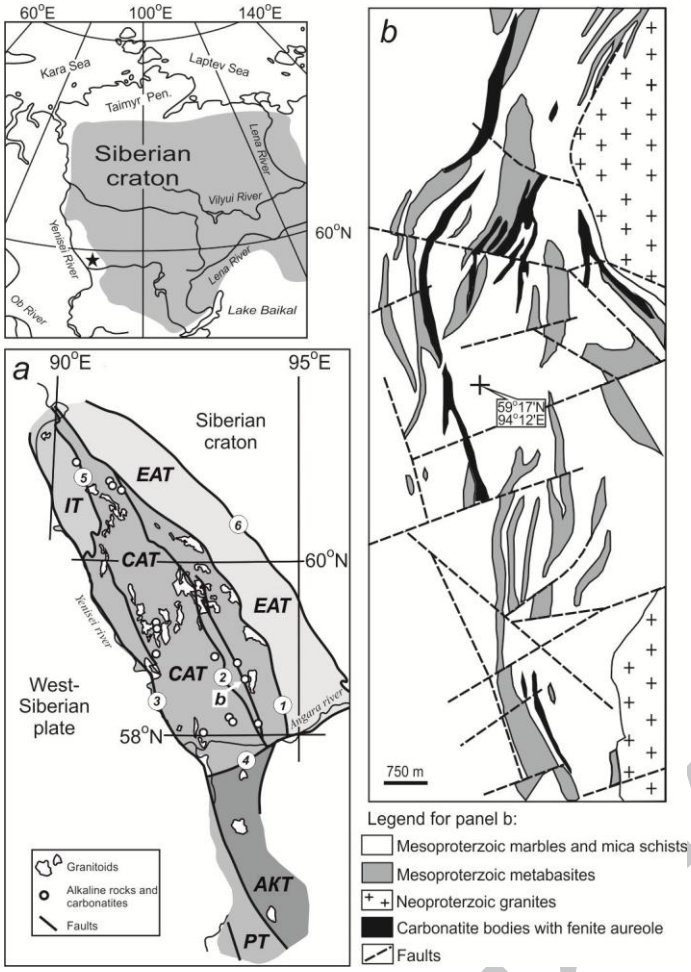

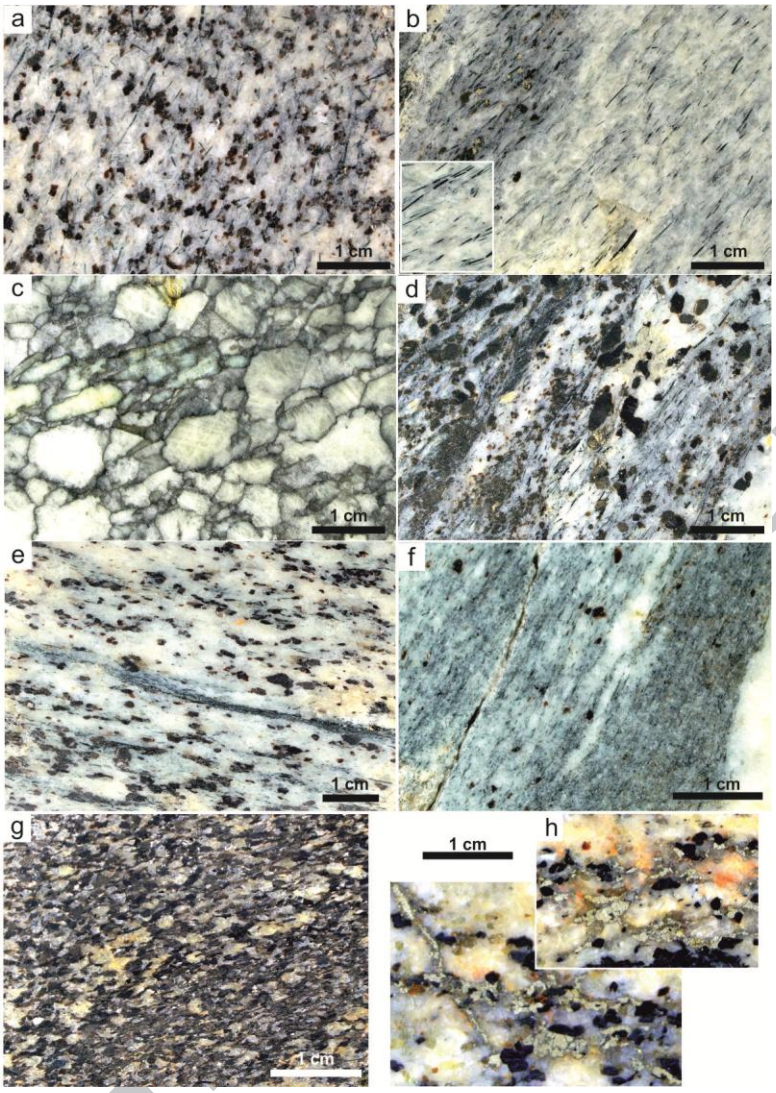

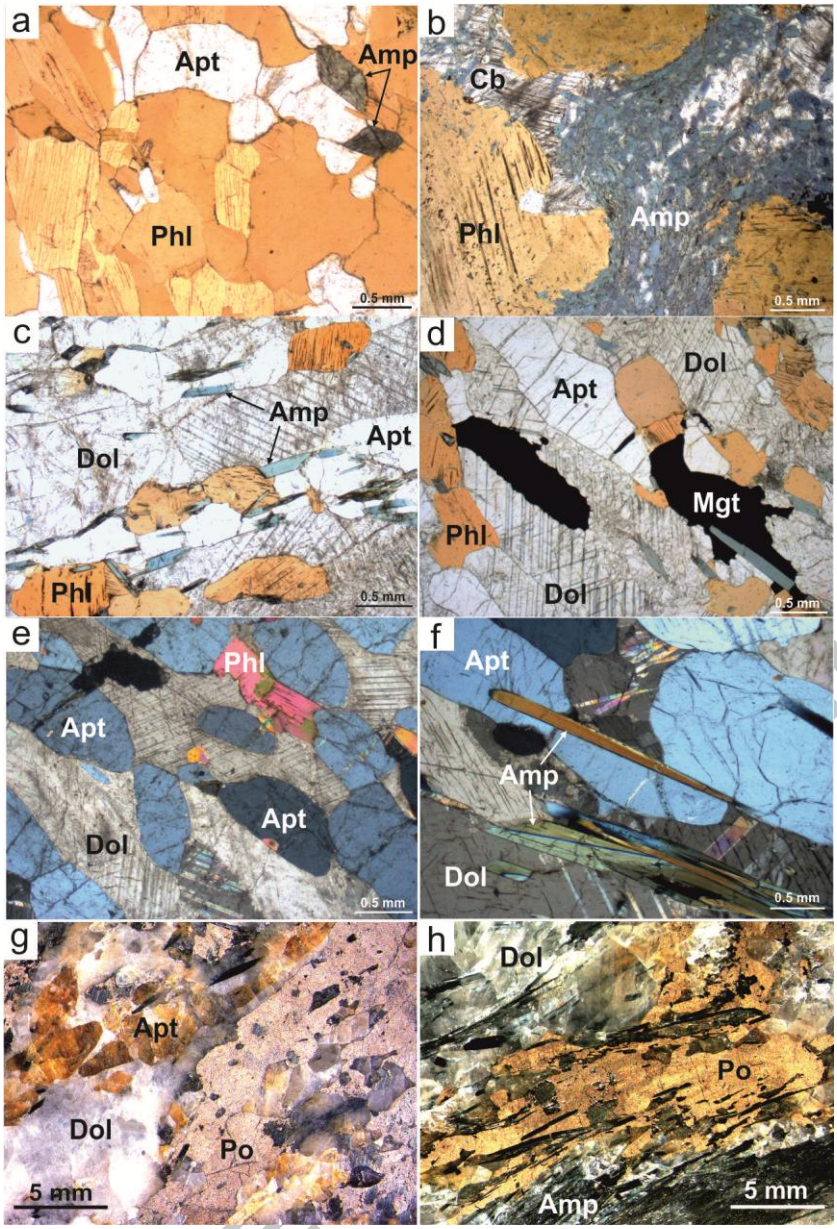

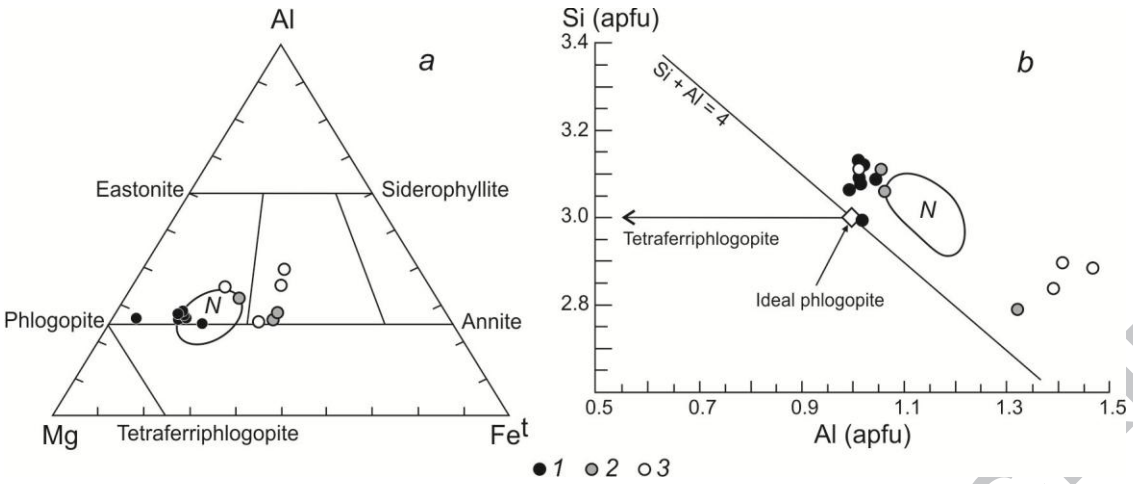

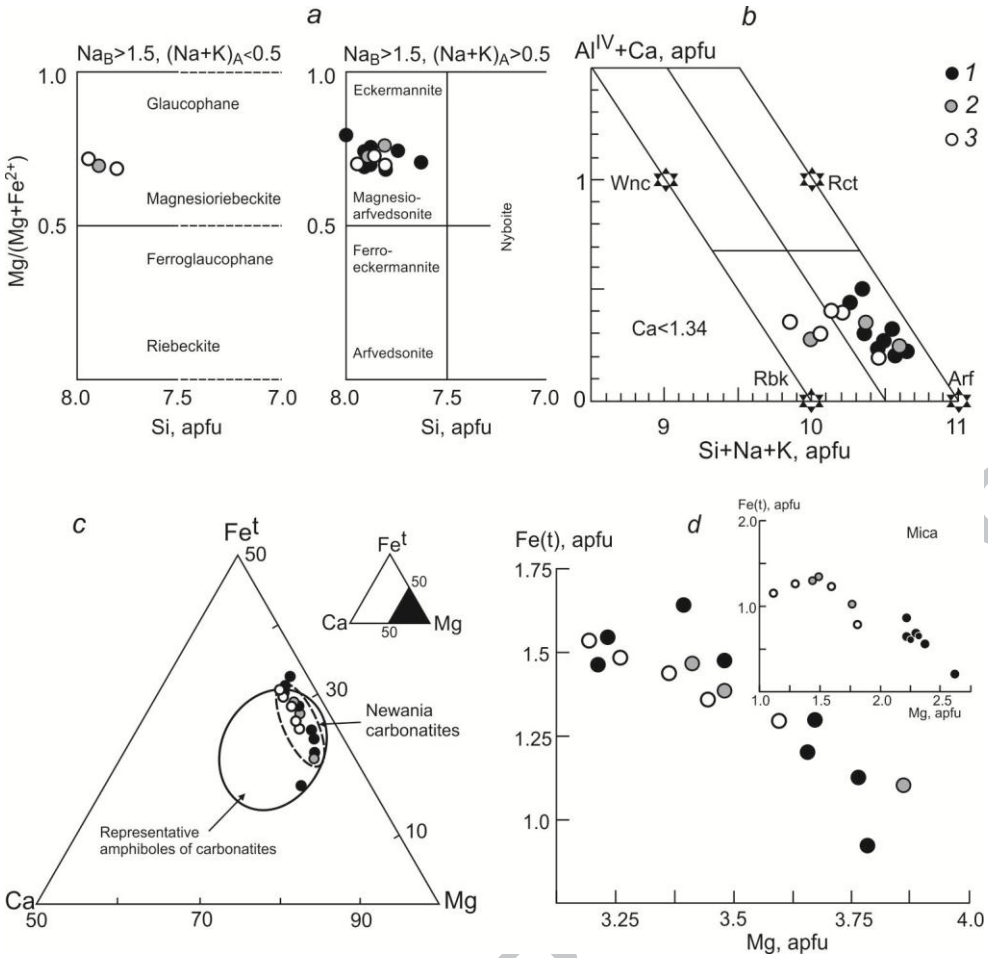

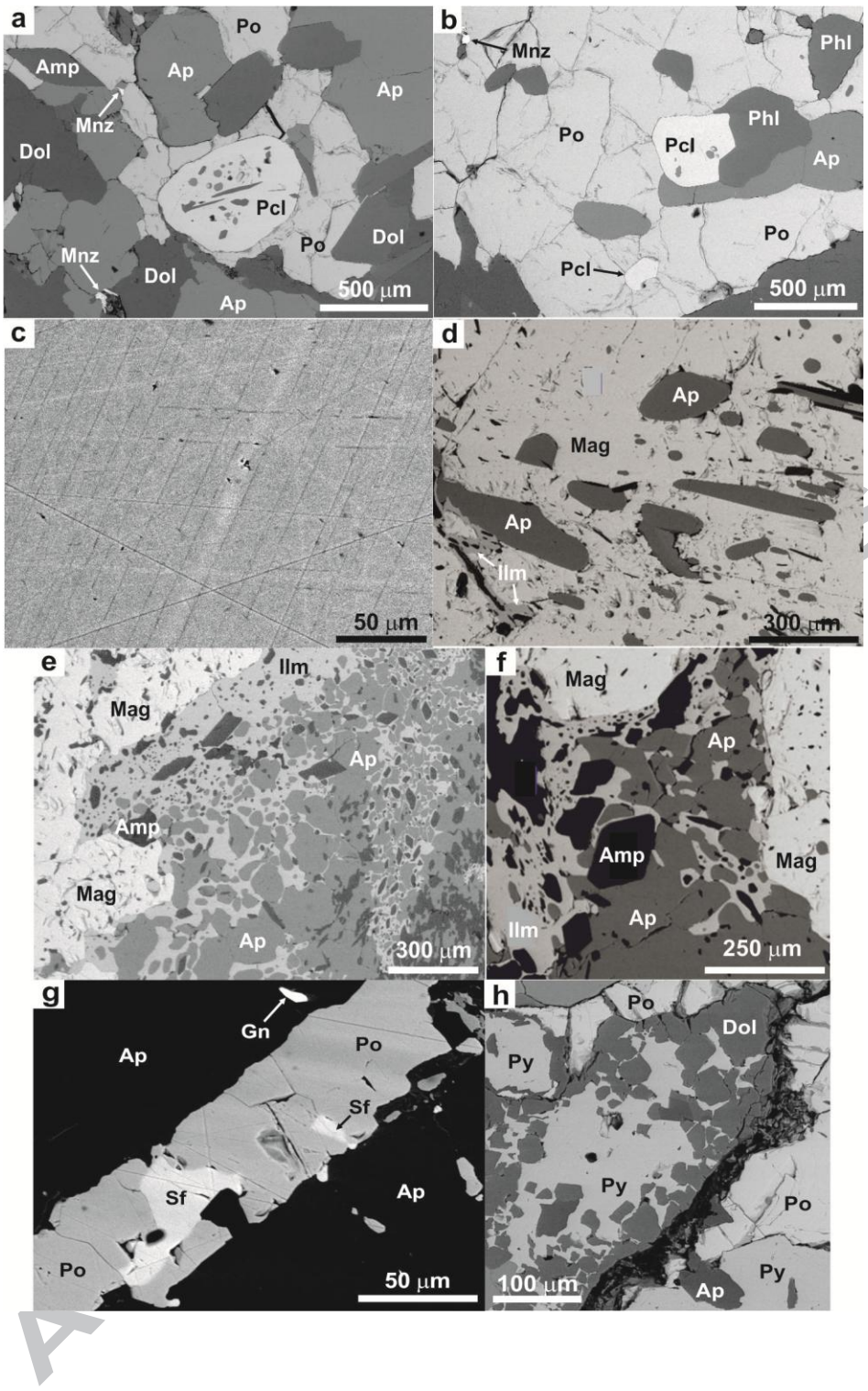

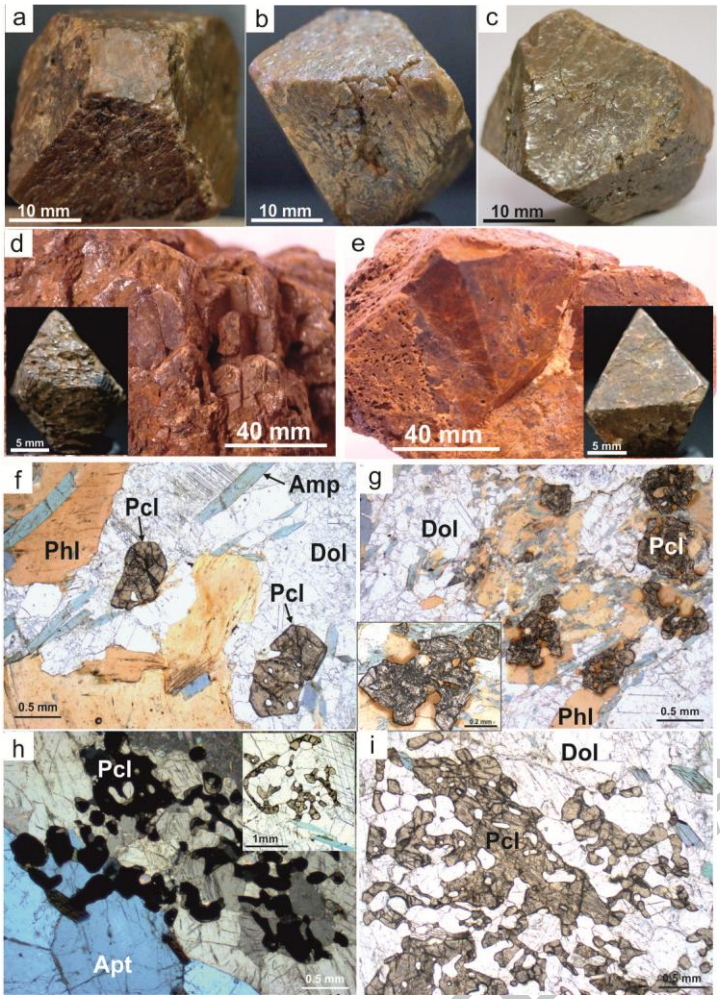

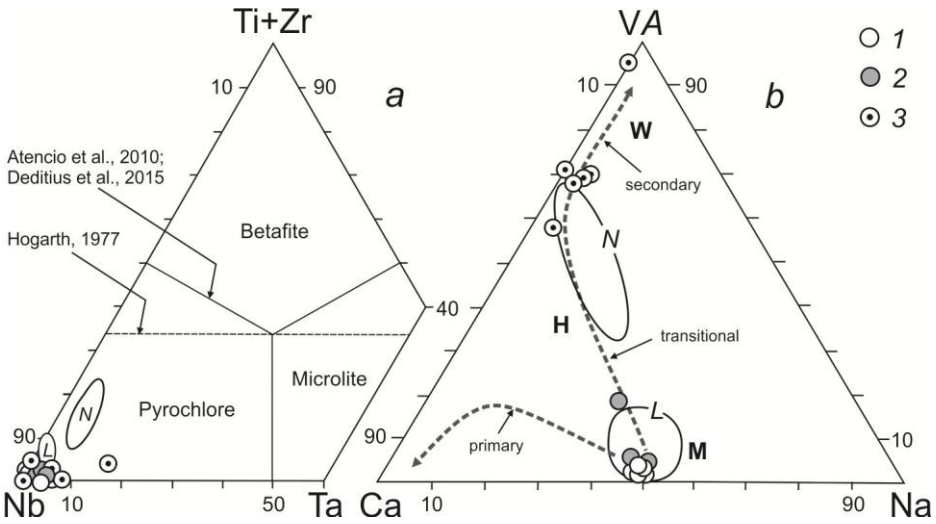

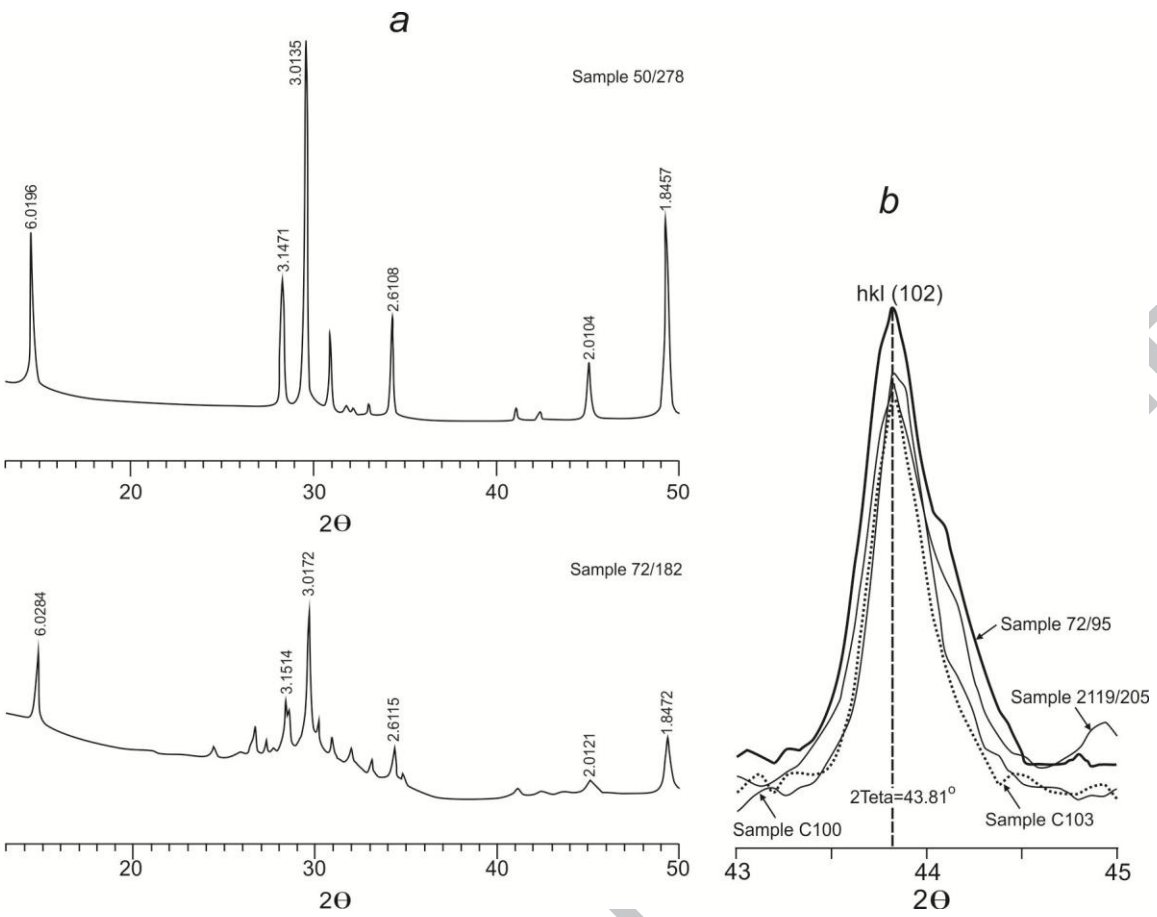

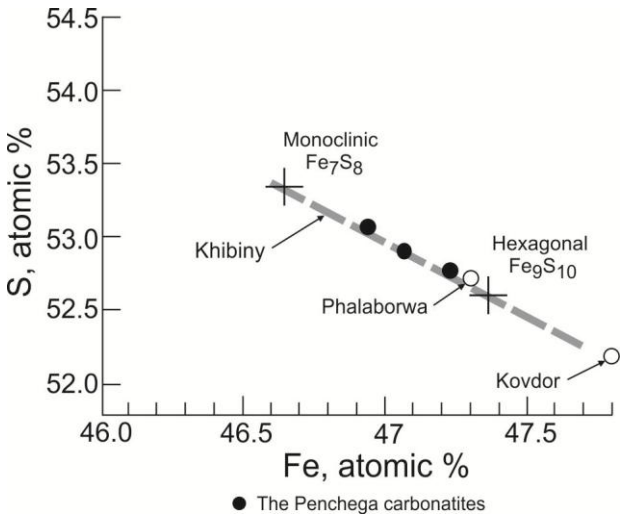

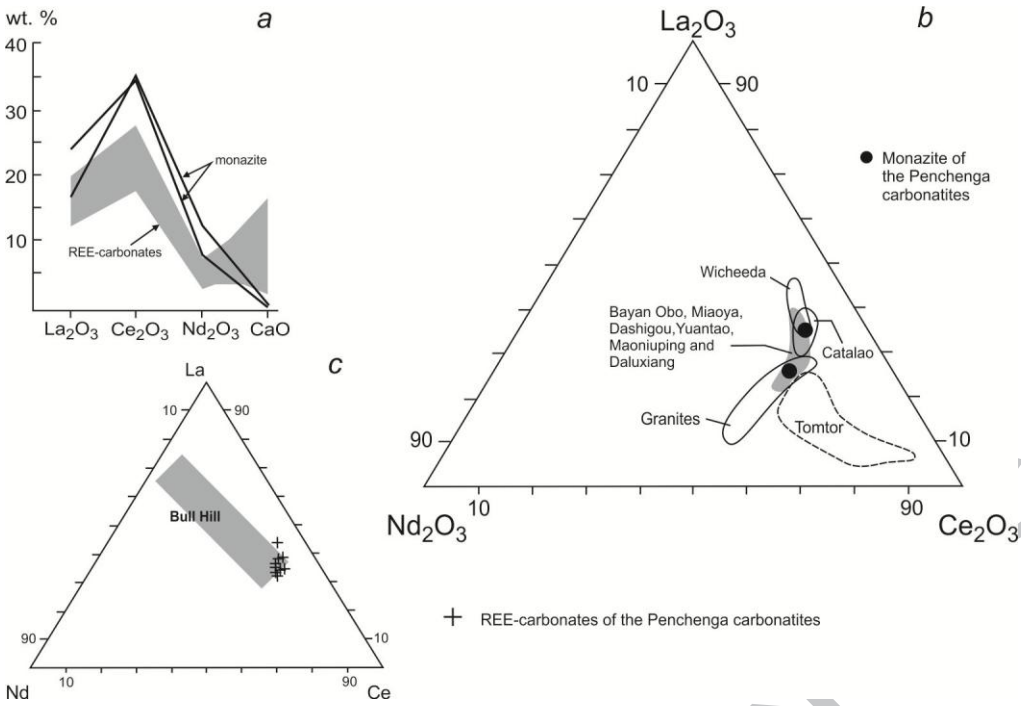

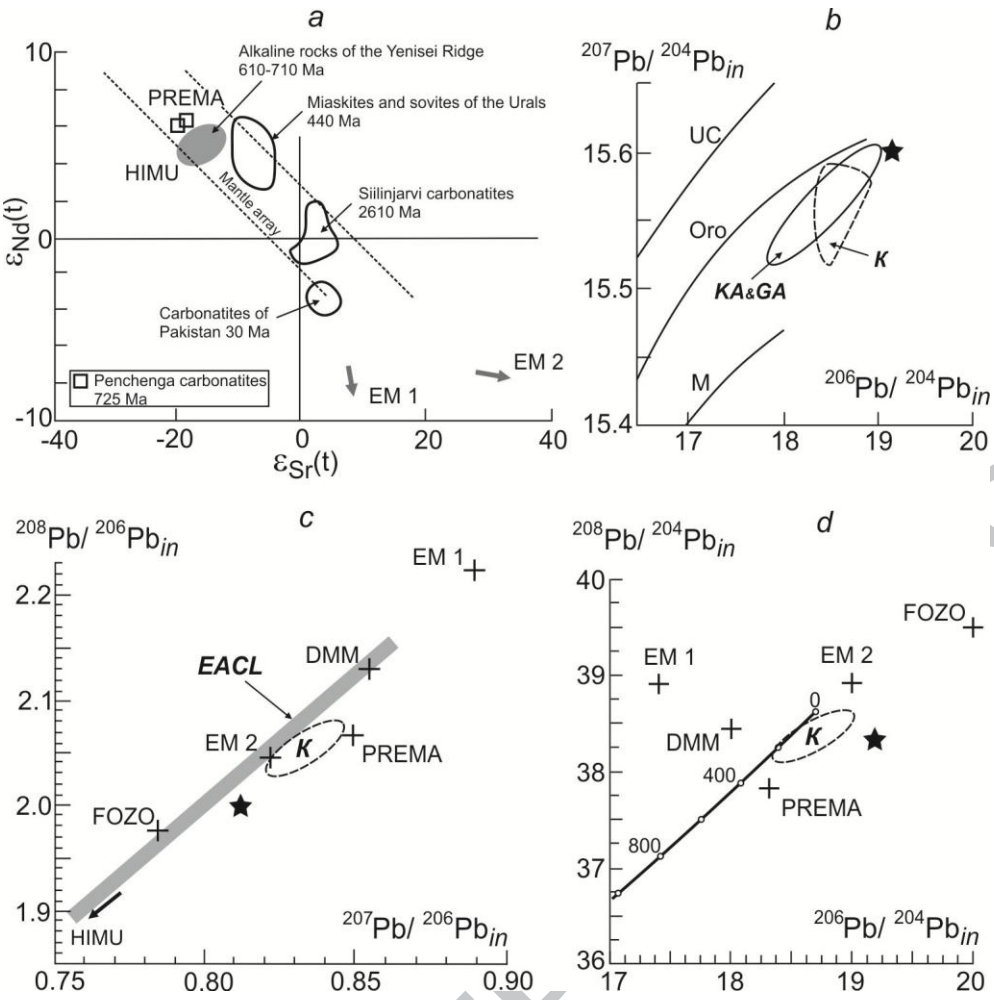

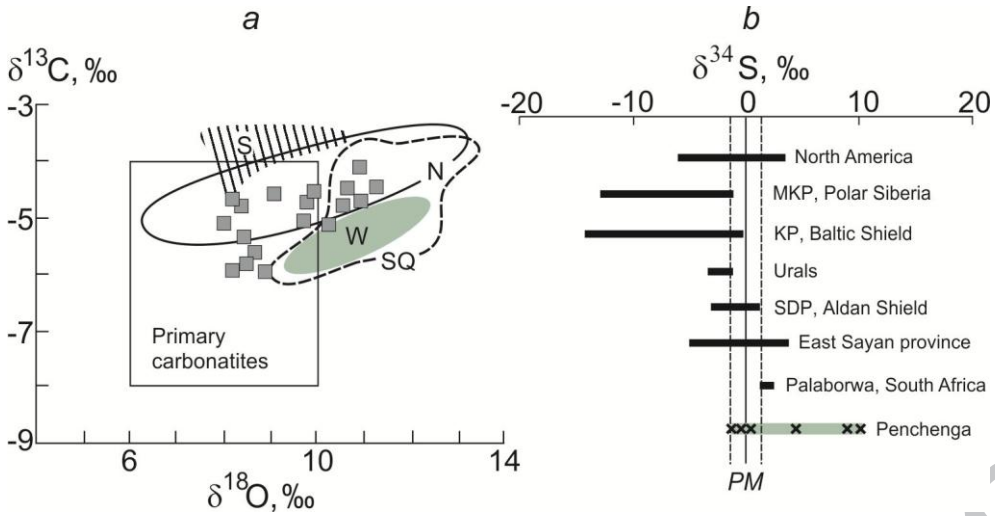

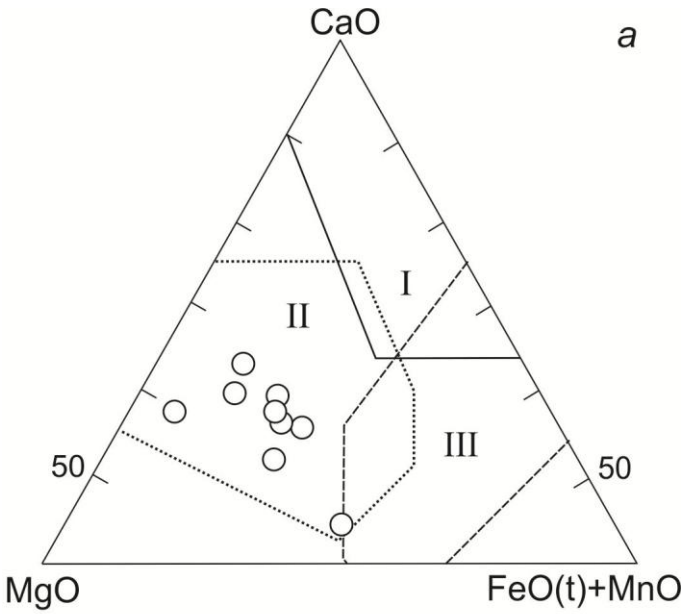

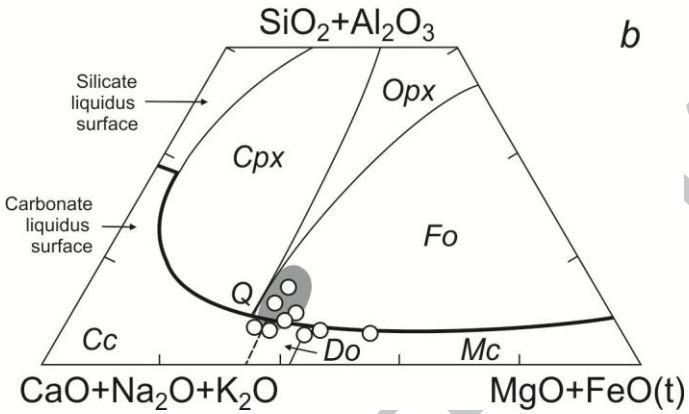

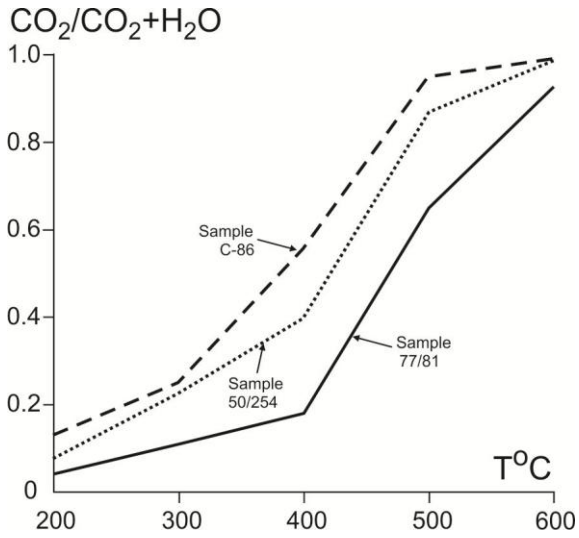

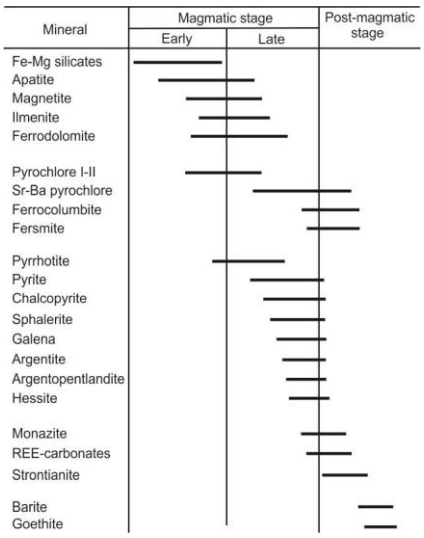

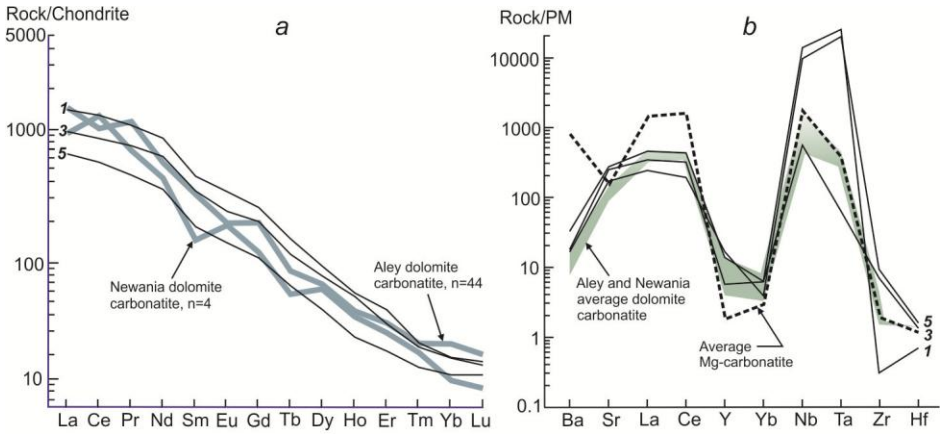

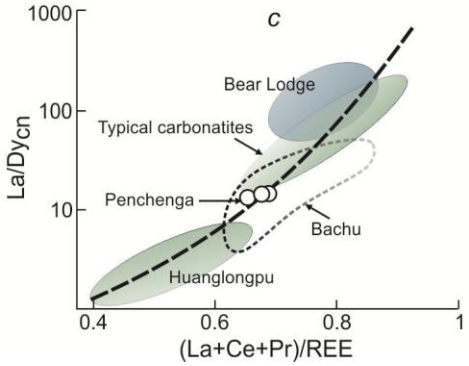

Penchenga carbonatite varieties:

1 - Pegmatitic (n=1)

3 - Banded trachytoid (n=3)

5 - Trachytoid (n=5)

Table 1
Representative major-element compositions of rock-forming Ca–Mg–Fe carbonates and strontianite,
Penchenga complex.

Mineral	Ferrodolomite									
										Av(34)
MgO, wt. %	20.67	21.21	18.19	17.60	17.95	17.21	17.13	19.08	17.87	18.55
CaO	32.64	31.08	32.33	32.75	31.86	33.28	31.47	31.99	32.46	32.21
MnO	0.93	0.88	1.57	1.63	1.44	2.24	1.71	1.43	1.86	1.52
FeOt	5.42	5.02	9.40	8.90	8.46	9.72	8.17	7.61	8.43	7.90
SrO	0.94	0.75	1.13	0.73	0.96	0.76	0.74	0.93	0.85	0.87
Total	60.60	58.94	62.62	61.61	60.67	63.21	59.22	61.04	61.47	

Table 1 (continued)

Mineral	Calcite						Strontianite		
						Av(13)			
MgO, wt. %	1.88	1.52	1.11	1.08	–	1.40	–	–	–
CaO	55.18	54.13	54.90	54.05	53.94	54.44	3.05	3.58	10.40
MnO	1.13	1.12	0.98	0.97	1.08	1.06	–	–	–
FeOt	1.78	1.65	1.64	1.13	1.47	1.53	–	0.10	–
SrO	1.61	1.91	1.82	1.71	1.84	1.78	63.56	69.12	61.02
Total	61.58	60.33	60.45	58.94	59.96[a]		68.06[b]	73.11[c]	73.46[d]

Table 1 (continued)

Mineral	Ankerite		Siderite			
MgO, wt. %	4.29	4.88	7.62	13.04	1.31	1.20
CaO	22.46	31.54	0.80	–	6.77	4.16
MnO	1.35	1.81	0.64	2.35	0.72	–
FeOt	37.87	26.50	59.05	53.47	61.09	63.43
Total	65.97	64.73	68.11	68.86	69.89	68.79

Note. [a] is 1.63 wt. % Na_2O. [b] is 1.45 wt. % BaO. [c] is 0.31 wt. % Na_2O. [d] is 2.04 wt. % BaO. (–) is below detection limit. Av=average composition; numerals in braces show number of analyses.

Table 2
Representative major-element compositions of mica, Penchenga carbonatites.

	1	2	3	4	5	6	7	8	9	10
Sample	77/81	C-100/1	133/290	C-100	72/172	2901/146	78/295	C-86	50/290	1729/37
SiO_2. wt. %	42.29	42.32	42.61	42.09	41.89	41.72	40.80	36.91	37.66	39.40
TiO_2	0.79	0.50	0.35	0.24	0.57	0.59	0.58	2.08	1.96	1.97
Al_2O_3	11.70	11.70	12.01	11.82	12.06	11.53	10.83	14.89	10.52	11.32
FeO(t)	3.12	9.18	10.37	10.12	9.33	9.79	13.41	16.06	19.66	19.90
MgO	23.72	21.78	20.89	20.75	20.37	19.95	20.29	15.50	12.17	11.91
Na_2O	0.24	0.13	0.15	0.22	0.26	0.29	–	0.02	–	–
K_2O	10.12	10.57	9.31	10.15	10.44	10.08	10.66	7.88	8.90	9.44
Total	91.98	96.18	95.69	95.39	94.92	93.95	96.57	93.34	90.87	93.94
Mg#	0.93	0.81	0.78	0.79	0.80	0.79	0.73	0.64	0.53	0.52
Mg/Fe(t)	13.7	4.3	3.6	3.7	3.9	3.7	2.7	1.7	1.1	1.1
Si, apfu	3.122	3.061	3.076	3.078	3.092	3.113	2.988	2.79	3.06	3.111
Ti	0.044	0.027	0.019	0.013	0.032	0.033	0.032	0.118	0.119	0.117
Al^{IV}	0.878	0.939	0.924	0.922	0.908	0.887	1.012	1.210	0.940	0.889
Al^{VI}	0.138	0.057	0.096	0.094	0.139	0.125	–	0.113	0.066	0.163
Mg	2.626	2.363	2.262	2.276	2.255	2.233	2.229	1.757	1.483	1.411
Fe^{2+}	0.192	0.553	0.624	0.617	0.574	0.609	0.818	1.011	1.331	1.310
Na	0.034	0.018	0.021	0.031	0.037	0.042	–	0.003	–	–
K	0.954	0.976	0.858	0.947	0.984	0.96	0.997	0.76	0.923	0.952
O=	0.335	0.166	0.088	0.177	0.315	0.306	–	–	0.288	0.459
OH=	1.665	1.834	1.912	1.823	1.685	1.694	2.031	2.098	1.712	1.541

Note. 1–7 = carbonatites; 8–10 = glimmerite shlieren at contacts of carbonatite bodies. Mg# = Mg/(Mg +ΣFe). Atoms per formula units (apfu) are based on 12 oxygens. (–) is below detection limit.

Table 3
Representative major-element compositions of mica and amphibole, Penchenga fenites.

Sample	50/287		2119/120		T-10		T-21		2901/90
Mineral	*Amp*	*Mica*	*Amp*	*Mica*	*Amp*	*Mica*	*Amp*	*Mica*	*Amp*
SiO_2. wt. %	56.69	37.71	57.12	36.53	55.35	40.59	55.6	36.93	56.33
TiO_2	0.08	3.13	0.04	6.46	0.18	1.29	0.15	2.88	0.20
Al_2O_3	0.92	15.62	1.12	15.80	1.88	11.21	1.99	15.25	0.77
FeO(t)	10.83	12.80	12.19	17.56	12.53	18.99	12.93	19.18	11.15
MgO	17.01	15.86	15.93	9.36	15.20	13.73	14.93	10.84	16.01
CaO	1.59	–	0.90	–	1.12	–	1.35	–	1.49
Na_2O	8.11	0.30	8.53	0.35	6.83	0.02	7.93	0.02	7.21
K_2O	0.90	9.27	1.10	9.46	0.86	8.64	0.76	8.77	0.71
Total	96.16	94.69	96.93	95.52	93.95	94.47	95.64	93.87	93.87
Mg#	0.74	0.69	0.70	0.49	0.69	0.57	0.68	0.50	0.72
Mg/Fe(t)	–	2.2	–	0.96	–	1.3	–	1.0	–
Si, apfu	7.834	2.842	7.943	2.885	7.809	3.117	7.800	2.896	7.935
Ti	0.008	0.177	–	0.383	–	0.074	–	0.169	–
Ti_C	–	–	0.004	–	0.019	–	0.016	–	0.022
Al^{IV}	0.152	1.158	0.057	1.115	0.191	0.883	0.200	1.104	0.065
Al^{VI}	–	0.227	0.128	0.353	0.126	0.129	0.133	0.302	0.065
Mg	3.591	1.793	3.357	1.109	3.259	1.581	3.191	1.275	3.442
Fe^{2+}	1.270	0.804	1.427	1.156	1.493	1.215	1.536	1.253	1.332
ΣC	4.861	–	4.917	–	4.897	–	4.876	–	4.860
Ca	0.240	–	0.135	–	0.172	–	0.206	–	0.229
Na_B	1.760	–	1.865	–	1.828	–	1.794	–	1.771
Na_A	0.449	0.044	0.455	0.053	0.061	0.003	0.393	0.003	0.229
K	0.162	0.892	0.197	0.954	0.157	0.847	0.138	0.878	0.130
ΣA	0.611	–	0.653	–	0.218	–	0.532	–	0.359
O=	–	0.358	–	1.010	–	0.244	–	0.418	–
OH=	–	1.642	–	0.990	–	1.756	–	1.582	–

Note. *Amp* = amphibole; *Mica* = dark mica. Mg# = Mg/(Mg +ΣFe). Atoms per formula units (apfu) of amphiboles are based on 23 oxygens. (–) is below detection limit.

Table 4
Representative major-element compositions of amphibole, Penchenga carbonatites.

	1	2	3	4	5	6	7	8	9	10	11
Sample	133/290	50/278	50/254	C-77	2901/146	77/81	C7-100	78/295	50/290	C-86	1729/37
SiO_2, wt. %	58.77	57.52	57.64	57.09	55.94	55.49	55.63	55.58	56.90	57.16	56.98
TiO_2	0.39	0.02	0.02	–	0.30	0.03	0.23	–	0.02	0.03	0.04
Al_2O_3	0.97	0.30	0.40	0.93	1.42	1.48	2.03	0.72	0.31	0.99	0.96
FeO(t)	5.94	9.64	10.30	11.36	12.31	12.70	12.86	13.90	9.46	11.82	12.36
MgO	19.67	17.89	17.47	17.74	14.87	14.99	16.63	15.91	18.30	16.50	16.19
CaO	2.96	1.66	1.40	1.11	1.13	0.84	1.14	0.58	1.92	1.00	1.07
Na_2O	7.49	8.21	8.63	9.72	8.25	9.12	9.65	9.27	8.52	9.29	7.00
K_2O	1.15	1.25	1.22	0.97	1.15	0.99	0.79	1.24	1.34	1.00	1.07
Total	97.34	96.49	97.08	98.92	95.37	95.64	98.96	97.20	96.77	97.79	95.67
Mg#	0.80	0.77	0.75	0.74	0.69	0.68	0.70	0.67	0.78	0.72	0.70
Si, apfu	8.071	7.910	7.937	7.775	7.938	7.908	7.607	7.812	7.813	7.904	7.891
Ti_T	–	0.002	–	–	–	–	0.024	–	0.002	–	–
Ti_C	0.040	–	0.002	–	0.032	0.003	–	–	–	0.003	0.004
Al^{IV}	–	0.049	0.063	0.151	0.062	0.092	0.331	0.120	0.051	0.096	0.109
Al^{VI}	0.157	–	0.002	–	0.178	0.158	–	–	–	0.066	0.049
Fe^{3+}	0.278	–	–	–	–	–	–	–	–	–	–
$Fe^{2+}{}_C$	0.680	1.126	1.201	1.306	1.475	1.523	1.484	1.639	1.107	1.378	1.444
Mg_C	3.774	3.761	3.666	3.670	3.208	3.236	3.455	3.377	3.853	3.462	3.405
ΣC	4.929	4.887	4.872	4.976	4.894	4.921	4.94	5.016	4.96	4.909	4.902
Ca	0.436	0.249	0.210	0.164	0.174	0.130	0.169	0.088	0.289	0.150	0.161
Na_B	1.564	1.751	1.790	1.836	1.826	1.870	1.831	1.912	1.711	1.850	1.839
Na_A	0.426	0.476	0.547	0.759	0.470	0.670	0.756	0.627	0.603	0.665	0.060
ΣB	2.000	2.000	2.000	2.000	2.000	2.000	2.000	2.000	2.000	2.000	2.000
K	0.202	0.224	0.218	0.171	0.211	0.182	0.140	0.224	0.240	0.179	0.192
ΣA	0.628	0.700	0.765	0.929	0.682	0.852	0.896	0.851	0.844	0.843	0.252

Note. 1–8 = carbonatites; 9-11 = glimmerite shlieren at contacts of carbonatite bodies. Atoms per formula units (apfu) are based on 23 oxygens. Mg# = Mg/(Mg +ΣFe). (–) is below detection limit.

Table 5
Representative major-element compositions of apatite and monazite-(Ce), Penchenga carbonatites.

Mineral	Apatite							Monazite-(Ce)	
Sample	50/287	50/290	72/95	78/295	C2119	C77		72/95	78/295
Na_2O, wt. %	0.10	0.08	0.14	0.07	–	0.25	–	–	–
CaO	52.80	52.98	52.36	52.41	52.75	52.20	53.03	0.82	0.48
SrO	2.16	1.36	2.58	2.45	2.47	2.53	1.77	–	1.29
La_2O_3	–	–	–	–	–	–	–	17.02	23.84
Ce_2O_3	–	–	–	–	–	–	–	35.43	35.28
Pr_2O_3	–	–	–	–	–	–	–	2.46	2.10
Nd_2O_3	–	–	–	–	–	–	–	12.26	7.61
P_2O_5	41.77	41.61	41.73	41.60	41.62	41.80	41.39	30.27	29.06
F	3.11	3.17	3.07	3.38	3.37	3.27	3.15	–	0.18
Total	99.94	99.28[a]	100.02[b]	99.91	100.21	100.05	100.72[c]	98.90[d]	99.84
Na, apfu	0.017	0.013	0.023	0.012	–	0.042	–	–	–
Ca	4.850	4.890	4.819	4.838	4.856	4.801	–	0.034	0.02
Sr	0.107	0.068	0.128	0.122	0.122	0.125	–	–	0.029
La	–	–	–	–	–	–	–	0.245	0.344
Ce	–	–	–	–	–	–	–	0.507	0.506
Nd	–	–	–	–	–	–	–	0.171	0.106
Pr	–	–	–	–	–	–	–	0.035	0.030
P	3.026	3.029	3.029	3.029	3.022	3.032	–	1.000	0.963
F	0.842	0.862	0.833	0.920	0.914	0.886	–	–	0.022
O=	0.062	–	0.015	–	0.013	0.025	–	–	–
OH=	0.095	0.187	0.153	0.132	0.075	0.090	–	–	–

Note. [a] is 0.10 wt. % FeO(t). [b] is 0.14 wt. % FeO(t). [c] is 0.41 wt. % FeO(t); 0.97 wt. % Ln_2O_3 (Lapin et al., 1987). [d] is 0.64 wt. % FeO(t). (–) is below detection limit. Atoms per formula units (apfu) are calculated according to the number of cations (8 for apatite and 2 for monazite).

Table 6
Representative major-element compositions of magnetite and related ilmenite, Penchenga carbonatites, sample 50/290.

Mineral	*Ilm*	*Mag*	*Ilm*	*Mag*	*Ilm*	*Mag*	*Ilm*	*Mag*	*Ilm*
MgO, wt. %	2.00	–	0.81	–	1.19	–	0.64	–	1.58
FeOt	40.72	92.39	42.96	93.13	42.26	93.37	44.19	92.97	40.01
MnO	4.93	–	3.50	–	4.19	–	2.87	–	4.78
TiO_2	51.95	0.52	51.84	0.47	53.11	0.40	52.07	0.35	52.48
Total	99.60	92.91	99.11	93.60	100.75	93.77	99.77	93.32	98.85
Fe, apfu	0.848	2.985	0.909	2.987	0.876	2.988	0.929	2.990	0.843
Ti	0.973	0.015	0.986	0.014	0.991	0.012	0.985	0.010	0.995
Mg	0.075	–	0.031	–	0.044	–	0.024	–	0.060
Mn	0.104	–	0.075	–	0.088	–	0.062	–	0.102

Note. *Ilm* = ilmenite; *Mag* = magnetite. (–) is below detection limit.

able 7
epresentative major-element compositions of pyrochlore group minerals, Penchenga carbonatites.

Sample	1	2	3	4	5	6	7	8	9	10	11	12	13	14
Na_2O, wt. %	8.14	7.84	7.90	7.95	8.00	7.88	7.47	6.16	0.49	0.41	–	0.72	–	0.67
CaO	14.86	14.90	15.04	14.83	14.65	14.46	14.55	13.79	7.87	6.47	5.28	4.93	1.05	7.58
BaO	–	–	–	–	–	–	–	–	6.16	4.28	8.29	6.13	9.84	–
SrO	–	–	–	–	–	–	–	–	7.64	7.26	6.70	5.08	6.51	5.96
FeO(t)	–	–	–	–	–	–	–	–	2.96	2.46	2.84	2.17	0.57	–
SiO_2	–	–	–	–	0.39	0.58	0.79	1.00	2.57	3.29	–	–	–	–
TiO_2	0.88	0.85	0.76	0.62	0.80	0.71	0.77	0.92	–	0.96	–	1.73	–	1.66
Nb_2O_5	71.04	71.49	72.27	70.78	70.58	69.26	68.61	67.19	61.46	60.29	59.39	52.39	73.06	72.33
Ta_2O_5	–	–	–	–	0.94	0.78	2.50	3.11	3.72	3.91	8.62	17.64	–	–
F	4.88	5.01	4.90	4.99	5.08	5.02	4.94	5.02	0.55	–	–	–	–	0.44
Total	99.80	100.09	100.87	99.17	100.44	98.69	99.63	97.19	93.42	89.33	91.12	93.72[a]	91.03	89.64[b]
Na, apfu	0.979	0.948	0.947	0.967	0.964	0.964	0.917	0.726	0.061	0.049	–	0.094	–	0.077
Ca	0.989	0.997	0.998	0.998	0.977	0.979	0.989	0.900	0.539	0.430	0.388	0.355	0.068	0.479
Ba	–	–	–	–	–	–	–	–	0.154	0.104	0.223	0.162	0.234	–
Sr	–	–	–	–	–	–	–	–	0.282	0.260	0.265	0.197	0.228	0.203
Fe^{2+}	–	–	–	–	–	–	–	–	0.158	0.127	0.162	0.122	0.029	–
ΣA	1.968	1.945	1.945	1.965	1.941	1.943	1.906	1.626	1.194	0.970	1.038	0.930	0.559	0.759
VA	0.032	0.055	0.055	0.035	0.059	0.057	0.094	0.374	0.806	1.030	0.962	1.070	1.441	1.241
Si	–	–	–	–	0.024	0.037	0.050	0.061	0.164	0.204	–	–	–	–
Ti	0.041	0.040	0.035	0.029	0.037	0.034	0.037	0.042	–	0.045	–	0.087	–	0.074
Nb	1.991	2.015	2.019	2.006	1.982	1.974	1.964	1.846	1.771	1.686	1.839	1.590	2.000	1.926
Ta	–	–	–	–	0.016	0.013	0.043	0.051	0.065	0.066	0.161	0.322	–	–
ΣB	2.032	2.055	2.054	2.035	2.059	2.058	2.094	2.000	2.000	2.001	2.000	1.999	2.000	2.000
F	0.957	0.988	0.958	0.990	0.998	1.002	0.990	0.965	0.111	–	–	–	–	0.082

ote. 1–5 = pyrochlore I from trachytic carbonatites; 6–8 = pyrochlore II from pegmatitic carbonatites; 9–12 = Sr-Ba pyrochlore III; 13, 14 = supergene Sr-a and Sr pyrochlore from weathered carbonatites. [a] is 2.93 wt. % UO_2, 0.04 apfu; [b] is 1.00 wt. % Ce_2O_3, 0.02 apfu. (–) is below detection limit. Atoms per rmula units (apfu) are based on $A_{2-m}B_2X_{6-w}Y_{1-n}{\cdot}pH2O$, where m=0–1.7, w=0–0.7, n=0–1, p=0–2 (Hogarth, 1977; Atencio et al., 2010). VA is number of acancies at the A-site.

Table 8
XRD data for pyrochlore and pyrrhotite, Penchenga carbonatites.

Mineral	Sample	hkl	*d*, *Å*	2Θ, grade	*I*, notional unit
Pyrochlore	50/278	111	6.01961	14.7092	25
		311	3.14710	28.3499	20
		222	3.01348	29.6290	100
		400	2.61081	34.3408	20
		511	2.01038	45.0810	10
		440	1.84568	49.3337	60
	72/182	111	6.02836	14.6948	30
		311	3.15136	28.3207	24
		222	3.01722	29.6079	100
		400	2.61147	34.3405	21
		511	2.01211	45.0577	9.0
		440	1.84716	49.3364	25
Pyrrhotite	72/95	100	2.98	30.88	5
		101	2.64	33.90	5
		102	2.06	43.81	10
		110	1.72	53.25	4
	2119/205	100	2.98	29.97	5
		101	2.643	33.91	5
		102	2.063	43.82	10
		110	1.72	53.24	4
	C103	100	2.97	29.99	5
		101	2.64	33.92	5
		102	2.06	43.83	10
		110	1.72	53.24	4
	C100	100	2.97	30.01	5
		101	2.64	33.93	5
		102	2.06	43.87	10
		110	1.72	53.24	4

Table 9
Representative major-elements of ferrocolumbite and fersmite, Penchenga carbonatites.

Sample	1	2	3	4	5	6
CaO, wt. %	0.69	–	0.11	–	–	15.95
MgO	1.72	2.23	0.24	–	–	–
FeO(t)	15.54	15.47	19.04	20.67	20.48	–
MnO	1.52	1.85	2.58	–	–	–
SiO_2	–	0.74	0.67	–	–	0.63
TiO_2	0.72	–	1.04	0.86	2.07	0.92
Nb_2O_5	77.23	79.05	74.19	79.25	77.98	78.30
Ta_2O_5	4.25	1.61	1.07	–	–	2.47
Total	101.67	100.95	98.94	100.78	100.53	98.27
Mg, apfu	0.141	0.182	0.021	–	–	–
Ca	0.040	–	0.007	–	–	0.932
Mn	0.070	0.085	0.126	–	–	–
Fe	0.709	0.700	0.919	0.947	0.929	–
ΣA	0.960	0.967	1.073	0.947	0.929	0.932
Si	–	0.040	0.039	–	–	0.034
Ti	0.030	–	0.045	0.035	0.085	0.038
Nb	1.907	1.936	1.938	1.965	1.915	1.926
Ta	0.063	0.024	0.017	–	–	0.037
ΣB	2.000	2.000	2.039	2.000	2.000	2.035

Note. 1-5 = ferrocolumbite from pegmatitic carbonatites (1, 2; sample 72/182), (3, after Lapin et al., 1987) and from weathered carbonatites (4, 5). 6 = fersmite, 1.74 wt. % Ce_2O_3, 0.03 apfu. (–) is below detection limit. Atoms per formula unit (apfu) are based on 6 oxygens.

Table 10

Representative major-element compositions of sulfides, Penchenga carbonatites.

Sample	1(29)	2(33)	3(22)	4(3)	5(12)	6(4)	7(23)	8(24)	9(13)	10	11(11)	12(4)	13(2)
S, wt. %	38.61	39.10	39.42	51.30	52.42	52.97	34.79	34.66	34.55	13.45	33.12	33.39	32.49
Fe	59.46	60.55	61.43	45.94	46.20	46.91	30.43	30.39	30.38	4.03	8.11	7.07	2.47
Cu	–	–	–	–	–	–	34.71	34.61	34.68	–	–	–	–
Pb	–	–	–	–	–	–	–	–	–	81.91	–	–	–
Zn	–	–	–	–	–	–	–	–	–	–	56.92	58.46	63.85
Cd	–	–	–	–	–	–	–	–	–	–	1.88	0.50	–
Total	98.07	99.65	100.85	97.24	98.62	99.88	99.93	99.66	99.61	99.39	100.03	99.42	98.81

Note. 1-3 = pyrrhotite; 4-6 = pyrite; 7-9 = chalcopyrite; 10 = galena; 11-13 = sphalerite. (–) is below detection limit. Numerals in braces are number of analyses.

Table 11
Representative major-element compositions of Ag-bearing sulfides and tellurides, Penchenga carbonatites.

Sample	1	2(3)	3(5)	4(2)
S, wt. %	11.63	32.80	30.68	0.34
Te	–	–	–	37.48
Fe	3.69	40.74	32.96	1.22
Cu	1.63	3.15	1.18	–
Ni	–	13.35	21.22	–
Ag	82.90	9.66	13.34	60.99
Total	99.85	99.70	99.38	100.03

Note. 1 = argentite; 2-3 = argentopentlandite; 4 = hessite. (–) is below detection limit. Numerals in braces are number of analyses.

Table 12
Chemical composition of synchysite-(Ce) and ancylite-(Ce) in carbonatites.

Mineral	Synchysite-(Ce)				Ancylite-(Ce)			
Complex	Penchenga		Wicheeda	Khibiny	Penchenga			W
Sample	C100/1(2)	C100сл(3)	(6)	604/413	C77(3)	C100/140	C7-100	(4
CaO, wt. %	16.25	14.91	16.09	16.89	2.80	2.10	3.57	2.6
SrO	1.61	1.06	0.58	0.43	17.48	19.60	21.83	15
BaO	–	1.79	–	0.15	–	–	–	–
FeOt	–	0.95	0.24	0.35	0.83	–	–	0.5
La_2O_3	20.08	19.35	17.28	15.06	18.33	16.81	14.92	17
Ce_2O_3	27.30	27.08	24.03	27.21	27.38	27.01	23.11	21
Nd_2O_3	6.16	6.80	6.41	7.90	6.46	7.14	5.88	4.1
F	6.79	6.03	5.91	5.69	0.13	0.86	0.84	–
Total	78.19	77.97	70.54	73.68	73.41	73.52	70.15	62
Ca, apfu	0.918	0.851	0.979	0.978	0.183	0.140	0.236	0.2
Sr	0.049	0.033	0.019	0.013	0.614	0.703	0.776	0.6
Ba	–	0.037	–	0.003	–	–	–	–
Fe(t)	–	0.042	0.011	0.016	0.042	–	–	0.0
Total	0.967	0.963	1.009	1.010	0.839	0.843	1.012	0.8
La	0.390	0.379	0.361	0.300	0.411	0.385	0.338	0.4
Ce	0.527	0.528	0.499	0.538	0.610	0.614	0.521	0.5
Nd	0.116	0.129	0.130	0.152	0.140	0.158	0.129	0.1
Total	1.033	1.036	0.990	0.990	1.161	1.157	0.988	1.1
F	1.131	1.015	1.060	0.971	0.025	0.169	0.163	–

Note. Atoms per formula units (apfu) are calculated by the number of cations. (–) is below detection limit. Numerals in braces are number of analyses. Ideal formula for synchysite: $Ca(Ce, La)(CO_3)_2F$. Ideal formula for ancylite: $Sr(Ce, La)(CO_3)_2(OH)\times H_2O$. Synchysite and ancylite from the Khibiny and Wicheeda carbonatites, after Zaitsev et al. (1998a) and Dalsin et al. (2015) respectively.

Table 13
Chemical composition of cordylite-(Ce) and cebaite-(Ce) in carbonatites.

Complex	Penchenga				Wicheeda		Khibiny	
Sample	1(2) C2-100	2(2) C100/1	3(3) C100сл	4 C100/1	5(7)	6(6)	7 603/165	8(18) 603/143
Na_2O, wt. %	2.85	3.03	1.89	–	0.66	–	2.56	–
CaO	4.25	4.26	4.59	1.72	2.87	0.52	4.10	0.61
SrO	4.37	6.27	5.68	3.19	3.72	1.55	5.90	1.43
BaO	23.70	24.41	26.43	41.02	21.87	41.21	23.11	42.77
La_2O_3	12.90	13.00	15.54	14.16	15.17	12.53	11.49	5.67
Ce_2O_3	18.14	19.57	20.25	15.57	19.33	14.49	17.90	14.45
Nd_2O_3	4.25	4.77	4.12	2.69	3.99	2.83	5.36	5.54
F	2.43	2.88	2.22	3.33	2.64	3.79	2.85	3.76
Total	72.89	78.44[a]	81.20[b]	81.68	70.25	76.92	73.27	74.23
Na, apfu	0.634	0.626	0.393	–	0.175	–	0.574	–
Ca	0.524	0.487	0.529	0.291	0.422	0.098	0.509	0.118
Ba	1.069	1.022	1.114	2.542	1.177	2.832	1.051	3.024
Total	2.227	2.135	2.036	2.833	1.774	2.930	2.134	3.142
La	0.546	0.511	0.615	0.824	0.766	0.808	0.490	0.376
Ce	0.763	0.764	0.796	0.900	0.970	0.929	0.759	0.953
Nd	0.175	0.182	0.158	0.152	0.195	0.177	0.222	0.357
Sr	0.290	0.386	0.352	0.291	0.294	0.157	0.395	0.149
Total	1.774	1.843	1.921	2.167	2.225	2.071	1.866	1.835
F	0.882	0.971	0.753	1.662	1.144	2.097	1.043	2.140

Note. 1-3, 5, 7 = cordylite; 4, 6, 8 = cebaite. [a] is 0.25 wt. % FeO(t); [b] is 0.48 wt. % FeO(t). Atoms per formula units (apfu) are calculated according to the number of cationic positions (4 for cordylite and 5 for cebaite). (–) is below detection limit. Numerals in braces are number of analyses. Ideal formulae are (Na, Ca)Ba(Ce, $La)_2(CO_3)_4F$ for cordylite-(Ce) and $Ba_3Ce_2(CO_3)_5F_2$ for cebaite-(Ce). Cordylite and cebaite from Khibiny and Wicheeda carbonatites, after Zaitsev et al. (1998a) and Dalsin et al. (2015) respectively.

Table 14
Sr–Nd isotopic composition for the Penchenga carbonatites.

Sample	Material	Sm (ppm)	Nd (ppm)	$^{147}Sm/^{144}Nd$	$^{143}Nd/^{144}Nd$	$^{143}Nd/^{144}Nd(t)$	$\varepsilon_{Nd}(t)$
50/278	Whole-rock	60.2	359	0.10147	0.512481	0.511999	5.79
	Amphibole	1.29	9.63	0.08103	0.512412	0.512027	6.33
	Pyrochlore	67.7	693	0.05901	0.512299	0.512019	6.18
50/254	Apatite	262	1487	0.10650	0.512517	0.512011	6.02
Sample	Material	Rb (ppm)	Sr (ppm)	$^{87}Rb/^{86}Sr$	$^{87}Sr/^{86}Sr$	$^{87}Sr/^{86}Sr(t)$	$\varepsilon_{Sr}(t)$
50/278	Amphibole	1.02	203	0.01460	0.702485	0.702334	–18.6
50/254	Apatite	0.17	12040	0.00004	0.702278	0.702278	–19.4

Note. Primary (T=725 Ma) isotope ratios, ε_{Nd} and ε_{Sr}, after (Vrublevskii et al., 2003, 2011).

Table 15
Pb isotopic composition of pyrrhotite, Penchenga carbonatites.

Sample	U (ppm)	Th (ppm)	Pb (ppm)	$^{206}Pb/^{204}Pb_m$	$^{207}Pb/^{204}Pb_m$	$^{208}Pb/^{204}Pb_m$	$^{206}Pb/^{204}Pb_{in}$	$^{207}Pb/^{204}Pb_{in}$	$^{208}Pb/^{204}Pb_{in}$
72/95	4.2	0.67	15	21.677	15.763	38.447	19.174	15.604	38.335

Note. U/Pb = 0.28, Th/Pb = 0.045. *m*=measured Pb isotopic ratios, *in*=initial (725 Ma) Pb isotopic ratios.

Table 16
Isotopic composition of O, C and H (in permil, ‰) and equilibrium temperatures for the minerals of Penchenga carbonatites

Rock (sample)	Mineral	$\delta^{13}C_{PDB}$	$\delta^{18}O_{SMOW}$	δD_{SMOW}	*T*, °C
Carbonatite	Dolomite	–4.5	10.6		
(77/81)	Arfvedsonite		4.1	–154	
	Phlogopite		3.8	–93	250
	Apatite		4.7		250
Carbonatite	Dolomite	–4.7	9.9		
(50/290)	Magnetite		–0.5		480
	Pyrochlore		–2.8		390
Carbonatite	Dolomite	–4.8	10.6		
(50/278)	Pyrochlore		–3.2		365
Carbonatite	Dolomite	–5.1	8.0		
(50/254)	Apatite		4.3		385
	Arfvedsonite		3.1	–98	
Carbonatite	Dolomite	–5.1	10.3		
(C100/1)	Phlogopite		5.1	–58	320
Carbonatite	Dolomite	–1.8	14.1		
(133/290)	Phlogopite		7.1	–30	240
Carbonatite	Pyrochlore		–3.2		
(T-1)	Magnetite		–0.3		
Fenite	Arfvedsonite		4.6	–102	
(50/287)	Phlogopite		4.9	–37	
Fenite	Arfvedsonite		5.0	–127	
(T-10)	Biotite		5.0	–67	
Fenite (T-21)	Biotite			–62	

Note. Data after Vrublevskii et al., 2003. Isotopic temperatures were calculated from the relationship: 1000 lnα (calcite-magnetite) = $5.91 \times 10^6/T^2$ (Chiba et al., 1989); 1000 lnα (calcite-apatite) = $1.6 \times 10^6/T^2$ (Fortier and Luttge, 1995); 1000 lnα (calcite-phlogopite) = $1.84 \times 10^6/T^2$ (Fortier et al., 1994); 1000 lnα (calcite-pyrochlore) = $5.61 \times 10^6/T^2$ (Mattews et al., 1983).

Table 17
Fluid phase composition (mg/kg) from micro-inclusions in apatite, Penchenga carbonatites.

Sample	Heating temperature, °C	CO_2	H_2O	CO	CH_4	Total	CO_2/ CO_2+H_2O
77/81	200	10	230	2	–	242	0.04
	300	20	160	3	–	183	0.11
	400	30	140	1	1	172	0.18
	500	130	70	4	3	207	0.65
	600	980	70	90	–	1140	0.93
C-86	200	10	70	0.7	–	80.7	0.13
	300	20	60	2	–	82	0.25
	400	50	40	0.7	0.2	90.9	0.56
	500	204	10	7	–	221	0.95
	600	990	10	60	–	1060	0.99
50/254	200	6	70	–	–	76	0.08
	300	10	30	1	–	41	0.25
	400	20	30	–	0.3	50.3	0.40
	500	130	20	4	–	154	0.87
	600	820	9	50	–	879	0.99

Table 18
Average major- and trace-element concentrations, Penchenga carbonatite varieties.

Rock type	Banded trachytoid (n=3)	Trachytoid (n=5)	Pegmatoid (n=1)
SiO_2, wt. %	5.11	2.67	3.67
Al_2O_3	0.60	0.16	0.43
Fe_2O_3	7.45	6.13	6.77
MnO	0.98	0.73	0.70
MgO	14.34	16.91	15.13
CaO	30.89	30.11	31.89
Na_2O	0.52	0.65	0.30
K_2O	0.67	0.11	0.19
P_2O_5	6.70	3.67	7.83
Ba, ppm	127	126	214
Sr	5348	3764	5898
Nb	404	6754	10266
Ta	2.3	1074	1168
Zr	77	104	3.3
Hf	0.43	0.44	0.2
Y	25	78	65
La	231	150	324
Ce	543	344	759
Pr	71	43	98
Nd	285	169	405
Sm	49	28	66
Eu	14	8.2	19
Gd	41	23	54
Tb	4.3	2.5	6
Dy	20	11	24
Ho	3	1.6	3
Er	5.7	3.5	7
Tm	0.57	0.38	0.6
Yb	3	1.9	3
Lu	0.37	0.28	0.4
ΣREE	1271	786	1769
LREE/HREE	15.3	16.8	17.1

Note. Data after Vrublevskii et al., 2003. Numerals in braces show number of analyses.

Graphical abstract

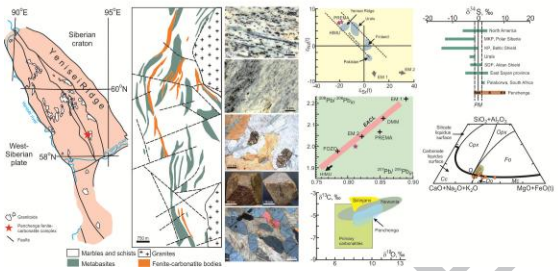

Highlights

► Neoproterozoic Penchenga magnesiocarbonatites of the Yenisei Ridge include magmatic accessory sulfide and rare-metal (Nb–Ta, REE) mineralization. ► The juvenile carbonatite melt was generated in a PREMA+EM 2-type mantle source. ► Isotope composition of minerals suggests inputs of continental crust material to the source of metals and interaction with meteoric waters.